**Roles of maternal *wnt8a* transcripts in axis formation in zebrafish**

Hiromu Hino[1,2], Akiko Nakanishi[1], Ryoko Seki[1], Tsubasa Aoki[2], Etsuro Yamaha[3], Atsuo Kawahara[4], Takashi Shimizu[1,2], and Masahiko Hibi[1,2]

[1]Laboratory of Organogenesis and Organ Function, Bioscience and Biotechnology Center, Nagoya University, Furo, Chikusa, Nagoya, Aichi 464-8601, Japan

[2]Division of Biological Science, Graduate School of Science, Nagoya University, Furo, Chikusa, Nagoya, Aichi 464-8602, Japan

[3]Nanae Fresh Water Laboratory, Field Science Center for Northern Biosphere, Hokkaido University, Nanae, Kameda, Hokkaido 041-1105

[4]Laboratory for Developmental Biology, Center for Medical Education and Sciences, Graduate School of Medical Science, University of Yamanashi, 1110 Shimokato, Chuo, Yamanashi 409-3898, Japan

Keywords: *wnt*, axis formation, maternal mutant, zebrafish

Correspondence: Masahiko Hibi
Laboratory of Organogenesis and Organ Function
Bioscience and Biotechnology Center, Nagoya University
Furo, Chikusa, Nagoya, Aichi 464-8601, Japan
Tel: +81-52-789-5198, Fax: +81-52-789-5053, E-mail: hibi@bio.nagoya-u.ac.jp

**ABSTRACT**

In early zebrafish development, the program for dorsal axis formation begins soon after fertilization. Previous studies suggested that dorsal determinants (DDs) localize to the vegetal pole, and are transported to the dorsal blastomeres in a microtubule-dependent manner. The DDs activate the canonical Wnt pathway and induce dorsal-specific genes that are required for dorsal axis formation. Among *wnt*-family genes, only the *wnt8a* mRNA is reported to localize to the vegetal pole in oocytes and to induce the dorsal axis, suggesting that Wnt8a is a candidate DD. Here, to reveal the roles of maternal *wnt8a*, we generated *wnt8a* mutants by transcription activator-like effector nucleases (TALENs), and established zygotic, maternal, and maternal zygotic *wnt8a* mutants by germ-line replacement. Zebrafish *wnt8a* has two open reading frames (ORF1 and ORF2) that are tandemly located in the genome. Although the zygotic ORF1 or ORF2 *wnt8a* mutants showed little or no axis-formation defects, the ORF1/2 compound mutants showed antero-dorsalized phenotypes, indicating that ORF1 and ORF2 have redundant roles in ventrolateral and posterior tissue formation. Unexpectedly, the maternal *wnt8a* ORF1/2 mutants showed no axis-formation defects. The maternal-zygotic *wnt8a* ORF1/2 mutants showed more severe antero-dorsalized phenotypes than the zygotic mutants. These results indicated that maternal *wnt8a* is dispensable for the initial dorsal determination, but cooperates with zygotic *wnt8a* for ventrolateral and posterior tissue formation. Finally, we re-examined the maternal *wnt* genes and found that Wnt6a is an alternative candidate DD.

## Introduction

Formation of the body axes, such as the dorso-ventral (DV) and antero-posterior (AP) axes, is one of the most important events in early vertebrate embryogenesis. In zebrafish, the animal (A)-vegetal (V) polarity of oocytes, which roughly corresponds to the AP axis in the embryo, is established during oogenesis (Langdon and Mullins, 2011). In contrast, no apparent DV axis is observed until the early gastrula stage, around 6 hours post fertilization (hpf), when the embryonic shield, which corresponds to the dorsal organizer, forms (Kimmel et al., 1995). However, evidence suggests that the developmental process for DV axis formation is initiated at the one-cell stage, soon after fertilization, in zebrafish. Approximately 20 minutes post fertilization (mpf), an array of parallel microtubules forms at the vegetal pole (Jesuthasan and Stahle, 1997; Tran et al., 2012). Disrupting the microtubules by nocodazol treatment, cold shock, or UV irradiation at this stage leads to loss of the embryonic shield and strong ventralization of the embryos (Jesuthasan and Stahle, 1997). Removal of the vegetal yolk mass at the early one-cell stage also results in severe ventralization of the embryos (Mizuno et al., 1999; Ober and Schulte-Merker, 1999). These data suggest that dorsal determinant(s) (DDs) localize to the vegetal pole and are transported along the vegetal microtubules to the future dorsal side. Consistent with this scenario, the plus ends of the vegetal microtubules are oriented to the future dorsal side, and vesicular structures (cortical granules) and some mRNAs are transported to the dorsal side in a microtubule-dependent manner (Ge et al., 2014; Tran et al., 2012).

Maternal-effect mutants of the genes that encode glutamate receptor interacting protein 2a (Grip2a, *hecate*), polypyrimidine-tract binding protein 1a (Ptbp1a, *brom bones*), and kinesin family member 5Ba (Kif5ba) have defects in the parallel microtubule array formation, and display severe ventralization. A maternal mutant of *syntabulin*, which encodes a motor protein linker that is involved in microtubule-dependent transport (Cai et al., 2005; Cai et al., 2007; Su et al., 2004), shows ventralization in a genetic background-dependent manner (Nojima et al., 2010; Nojima et al., 2004). All of these data also support the hypothesis that the microtubule-dependent transport of DDs plays an essential role in the initial dorsal determination.

The canonical Wnt pathway, which induces an accumulation of β-catenin, is known to play a pivotal role in dorsal determination in both *Xenopus* and zebrafish. Activation of the canonical Wnt pathway causes an ectopic formation or expansion of the dorsal organizer, while its inhibition leads to impaired dorsal axis formation [reviewed in (Hibi et al., 2002; Langdon and Mullins, 2011; Schier and Talbot, 2005)]. The maternal-effect mutant *ichabod*, which is defective in maternal β-catenin 2 expression, displays severe ventralization (Bellipanni et al., 2006; Kelly et al., 2000). In wild-type zebrafish, the nuclear accumulation of β-catenin is detected in dorsal blastomeres by the 128-cell stage, and in the dorsal blastoderm and dorsal yolk syncytial layer (YSL) at the mid-blastula stage (Dougan et al., 2003; Schneider et al., 1996). The dorsal-specific homeobox gene *dharma* (*bozozok*) and the Nodal-related gene *ndr1* (*squint*) function downstream of the canonical Wnt pathway to induce the

dorsal organizer (Fekany et al., 1999; Kelly et al., 2000; Leung et al., 2003; Ryu et al., 2001; Shimizu et al., 2000; Yamanaka et al., 1998). These data suggest that DDs activate the canonical Wnt pathway to induce dorsal-specific genes that are required for dorsal-organizer and dorsal-tissue formation.

In *Xenopus*, maternal Wnt11 is reported to activate the canonical Wnt pathway (Tao et al., 2005), and a complex of Wnt11 and Wnt5a has been suggested to serve as the DD (Cha et al., 2008; Cha et al., 2009). In zebrafish, neither *wnt11* nor *wnt5a* activates the canonical Wnt pathway or induces the expression of dorsal-specific genes (Lu et al., 2011; Nojima et al., 2010). Among the *wnt* genes in zebrafish, only the mRNA of *wnt8a* is reported to localize to the vegetal pole of oocytes (Lu et al., 2011). *wnt8a* mRNA is translocated in a microtubule-dependent manner (Ge et al., 2014; Lu et al., 2011; Tran et al., 2012). The expression of a dominant-negative Wnt8a inhibits expression of the dorsal-specific gene *chordin,* and the injection of *wnt8a* RNA rescues the dorsal-axis formation defect in microtubule-defective (nocodazol-treated) embryos (Lu et al., 2011). Thus, *wnt8a* mRNA (or Wnt8a protein) is so far the only candidate DD in zebrafish. The Zebrafish *wnt8a* gene has two ORFs that are tandemly located (Lekven et al., 2001). As zygotic *wnt8a* plays an essential role in posterior and ventral tissue formation, loss-of-function mutations of *wnt8a* ORF1 and ORF2 by either a deletion in the chromosomal that removes the *wnt8a* gene (chromosomal deletion) or antisense morpholino (MO)-mediated knockdown results in severe antero-dorsalization and embryonic lethality (Lekven et al., 2001; Shimizu et al., 2005), making it difficult to study the maternal function of *wnt8a* in zebrafish.

In this study, we generated *wnt8a* ORF1 and ORF2 single mutants, and ORF1/2 compound mutants by transcription activator-like effector nucleases (TALENs). We also generated maternal and maternal-zygotic *wnt8a* mutants by germ-line replacement (Ciruna et al., 2002; Saito et al., 2010). Our findings suggested that maternal *wnt8a* is dispensable for the initial dorsal determination, but functions cooperatively with zygotic *wnt8a* in ventrolateral and posterior tissue formation. We also demonstrated that maternal Wnt6a is an alternative DD candidate and may cooperate with maternal Wnt8a for the initial dorsal determination.

## Material and methods

### *Ethics statement*

The animal work in this study was approved by the Nagoya University Animal Experiment Committee (approval numbers 2014020503, 2015022304, 2016022203, and 2017030202) and was conducted in accordance with the Regulations on Animal Experiments at Nagoya University.

### *Zebrafish strains and husbandry*

Wild-type zebrafish (*Danio rerio*) with the Oregon AB genetic background were used. The allele names of the *wnt8a* mutants are designated in ZFIN (http://zfin.org) as follows: *wnt8a*$^{\Delta O1\text{-}1}$ and *wnt8a*$^{\Delta O1\text{-}2}$ are *wnt8a*$^{nub14}$ and *wnt8a*$^{nub15}$; *wnt8a*$^{\Delta O2\text{-}1}$, *wnt8a*$^{\Delta O2\text{-}2}$, and *wnt8a*$^{\Delta O2\text{-}3}$ are *wnt8a*$^{nub16}$, *wnt8a*$^{nub17}$, and *wnt8a*$^{nub18}$; *wnt8a*$^{\Delta O1\Delta O2\text{-}1}$,

*wnt8a*$_{\Delta O1\Delta O2\text{-}2}$, and *wnt8a*$_{\Delta O1\Delta O2\text{-}3}$ are *wnt8a*$_{nub19}$, *wnt8a*$_{nub20}$, and *wnt8a*$_{nub21}$; and *wnt8a*$_{del}$ is *wnt8a*$_{nub22}$. Zebrafish were maintained in environmentally controlled rooms at the Bioscience and Biotechnology Center, Nagoya University. Zebrafish embryos were incubated in embryonic medium (Westerfield, 1995) at 28.5 $^{o}$C.

*Generation of wnt8a mutants by TALENs and genotyping*

The TALENs were designed with the web software TALEN Targeter (https://tale-nt.cac.cornell.edu/node/add/talen) (Cermak et al., 2011) to introduce mutations into ORF1 (one region) and ORF2 (two regions) of zebrafish *wnt8a*. The TALENs for ORF1 contained the following repeat variable di-residues (RVDs): NN NN NG NI NG NI NN NI NI NN NI NN NG NN HD and NG HD HD NI HD HD NG NN NG HD HD HD NI NG, which recognized 5'-GGTATAGAAGAGTGC-3' and 5'-TCCACCTGTCCCAT-3', respectively. The first TALENs for ORF2 contained the RVDs: NI NN NI NG NN NG HD NI NG NN NN HD NI NG and HD HD NI NN HD NI NG NN NG NG NG NN HD NI NG NG, which recognized 5'-AGATGTCATGGCAT-3' and 5'-CCAGCATGTTTGCATT-3', respectively. The second TALENs for the ORF2 contained the RVDs: NN NN HD NI NG NN NG HD NI NN NI NI NI NN NG and HD NI NN HD ND NI NN NG NG NN HD NI NG HD HD NI NN HD, which recognized 5'-GGCATGTCAGAAAGT-3' and 5'-CAGCCAGTTGCATCCAGC-3', respectively. The TALEN cDNAs were constructed as described previously (Sakuma et al., 2013) and subcloned into pCS2pTAL3DD and pCS2TALRR (Dahlem et al., 2012). Capped RNAs were

synthesized as described below. One nL of solution containing a pair of TALEN RNAs (0.4 μg/mL each) was injected into zebrafish embryos at the one-cell stage. Insertion and/or deletion (indel) mutations were detected by heteroduplex mobility analysis (HMA) (Ota et al., 2013). The following primers were used for genotyping: 5'-CAGAGTGGTATAGAAGAGTGCA-3' (ORF1-F1) and 5'-CGCTTTCCGGGCAGTTCCACCT-3' (ORF1-R1) to detect the *wnt8a* ORF1 mutation in *wnt8a*$^{\Delta O1\text{-}1}$; 5'-GCAGTGTACAAGCTGGGGCT-3' (ORF1-F2) and 5'-AACTGCAGTGCGCTTTCCGG-3' (ORF1-R2) to detect the ORF1 mutations in *wnt8a*$^{\Delta O1\text{-}2}$ and *wnt8a*$^{\Delta O1\Delta O2\text{-}1,2,3}$; 5'-AAGCGACAATGAAGAAGGATTTGTAG-3' (ORF2-F1) and 5'- GGTAATTGCCAATCTCACGG-3' (ORF2-R1) to detect the *wnt8a* ORF2 mutations in *wnt8a*$^{\Delta O2\text{-}1,2,3}$; and 5'-GAGGATTTGTAGATGTCATGGCATG-3' (ORF2-F2), and ORF2-R1 to detect the ORF2 mutations in *wnt8a*$^{\Delta O1\Delta O2\text{-}1,2,3}$. The PCR products were separated on 12% TBE (Tris-borate-EDTA) acrylamide gels. To distinguish between wild-type and *wnt8a*$^{del}$ alleles, the primers ORF2-F2 and ORF2-R1 were used to detect the wild-type allele, and the primers ORF1-F2 and ORF2-R1 were used to detect the long deletion. The PCR products were separated on 3% TAE (Tris-acetate-EDTA) agarose gels.

*Germ-line replacement*

Germ-line replacement was performed by a modification of a previously published method (Ciruna et al., 2002; Saito et al., 2010). Donor embryos were obtained by crossing heterozygous *wnt8a* mutant male and female fish, and two nL of the following

solution: 0.5 μg/μl capped *GFP-Buc* (zebrafish *bucky ball*) RNA, 1% rhodamine-dextran (Thermo Fisher Scientific), and 0.2 M KCl was injected into the donor embryos at the one-cell stage. Into the host embryos was injected one nL of 1 μg/μL *dead end* (DND microRNA-mediated repression inhibitor 1, *dnd1* in ZFIN) antisense MO1 oligonucleotide (MO1-dnd1 in ZFIN) and 0.2 M KCl at the one-cell stage (Ciruna et al., 2002). At around the 16-cell (sphere) stage, the embryos were dechorionated by pronase treatment (Nacalai Tesque), loaded on a 1.5% agarose gel, and overlaid with Ringer solution containing 20 units/mL Ampicillin (Meiji Seika) and 100 μg/mL Spectinomycin (Meiji Seika). Blastomere cells that included Bucky Ball-GFP$^{+}$ rhodamine$^{+}$ cells were collected from sphere-stage donor embryos and transplanted into the animal pole of sphere-stage host embryos. The transplanted embryos were incubated in embryonic medium (Westerfield, 1995) containing antibiotics for one day, and the embryos with rhodamine$^{+}$ cells at the genital ridge were selected. After genotyping the donor embryos, the fish containing transplanted homozygous *wnt8a* mutant cells were further reared. The transplant-containing fish were treated with 100 ng/L estradiol (E2, Sigma-Aldrich) from 20 to 50 days post-fertilization to increase the proportion of female fish, as described previously (Saito et al., 2008).

*In situ hybridization*

The *noto* (formerly called *floating head*), *tbx6l* (*tbx6*), *otx2*, *chordin*, *goosecoid* (*gsc*), and *dharma* transcripts were detected as described previously (Lekven et al., 2001;

Shimizu et al., 2005; Yamanaka et al., 1998). To detect *wnt6a* and *wnt7ab* transcripts, the cDNAs were amplified from a maternal cDNA library with primers 5'-ATGATTGGCACTGGGAGTGG-3' and 5'-TGAGAGCATGTCTGGCACTG-3' for *wnt6a*, or primers 5'-CTCATGACAATGGCTGGA-3' and 5'-CCTCGGCCACAACACA-3' for *wnt7ab* and subcloned into pTAC2 (BioDynamics Laboratory Inc.). Whole-mount *in situ* hybridization was performed as described previously (Thisse and Thisse, 1998), except that the hybridization was performed at 65 $_{o}$C. BM purple AP substrate (Roche) or NBT/BCIP (Roche) was used as a substrate for alkaline phosphatase. Images were captured using an AxioPlan2 microscope equipped with an AxioCam CCD camera (Zeiss). The figures were constructed using Adobe Photoshop and Adobe Illustrator.

*Reverse transcription (RT)-PCR*

Total RNA was isolated from unfertilized oocytes using TRI Reagent (Molecular Research Center, Inc.) according to the manufacturer's protocol. Half of the total RNA from single oocytes (around 100 ng, Fig. 3C) or one μg of total RNA (Fig. 5) was used to generate cDNA in 20 μL of solution using ReverTra Ace (Toyobo). The cDNA was then subjected to semi-quantitative PCR. Primers for the *wnt8a* ORF1 and ORF2 were the same as those used for the genotyping of *wnt8a*$_{\Delta O1\Delta O2\text{-}2}$. The primers for *wnt6a* were 5'-ATCAGGCAGCGAAAGGGCAA-3' and 5'-TGACGGAAGAGCGGCATCTT-3'; and for *wnt7ab* were 5'-CTCATGACAATGGCTGGA-3' and 5'-CCTCGGCCACAACACA-3'; the primers for the other *wnt* genes were described

previously (*wnt6* and *wnt7a* were renamed *wnt6b* and *wnt7aa*, respectively, in ZFIN) (Lu et al., 2011). The *wnt8a* ORF1 and ORF2 were amplified from one μL of the cDNA using GoTaq DNA polymerase (Promega) with an annealing temperature of 54 $^{o}$C and 35 cycles. *wnt2bb* and *wnt7aa* were amplified from one μL of the cDNA using GoTaq DNA polymerase with an annealing temperature of 60 $^{o}$C and 35 cycles. *wnt7ab* and *wnt16* were amplified from 0.1 μL of the cDNA using GoTaq DNA polymerase with an annealing temperature of 55 $^{o}$C and 35 cycles. *wnt10b*, *wnt11*, and *wnt11r* were amplified from 0.1 μL of the cDNA using KOD Fx Neo DNA polymerase (Toyobo) with an annealing temperature of 68 $^{o}$C and 38 cycles. The other *wnt* genes were amplified from one μL of the cDNA by using GoTaq DNA polymerase with an annealing temperature of 60 $^{o}$C and 35 cycles.

*RNA injection*

The pCS2+ expression plasmids for *GFP-buc* (Saito et al., 2014), *wnt8a ORF1* (Lekven et al., 2001), *dkk1b* (Hashimoto et al., 2000), and *ΔN-tcf7l1a* (*tcf7l1a* was formerly called *tcf3a*) (Dorsky et al., 2003) were previously described. To construct an expression plasmid for *wnt6a*, the cDNA was amplified from the maternal cDNA library with primers: 5'-GGGGAATTCGCCGCCATGCTTTCAAAGCAAAAGCACG-3' and 5'-GGGTCTAGATTACAAGCAGAGGCTGACATTC-3', and after digestion with *EcoR*I and *Xba*I, the DNA fragment was subcloned into pCS2+. The pCS2+bucky ball-GFP was a gift from K. Inoue. To make synthetic RNAs for these genes, the plasmids were linearized with *Not*I. RNAs for *GFP-buc* and *ΔN-tcf7l1a* were

transcribed with SP6 RNA polymerase (Promega) in the presence of G(5')ppp(5')G RNA cap structure analog (New England BioLabs Inc.). To make capped and polyadenylated RNAs for *wnt6a*, *wnt8a*, and *dkk1b*, RNAs were transcribed with SP6 RNA polymerase in the absence of the cap structural analog, and then the RNAs were capped and polyadenylated using the ScriptCap™ m7G Capping System (Epicentre) and the A-Plus Poly(A) Polymerase Tailing Kit (Epicentre) according to the manufacturer's protocols. After ethanol precipitation, the RNA was dissolved in 0.2 M KCl solution. The RNAs were injected into early one-stage embryos (less than 20 min post fertilization), and the treated embryos were incubated in the embryonic medium (Westerfield, 1995).

*Statistics*

Data were analyzed for statistical significance by a chi-square test or one-way ANOVA with Dunnet's post-hoc test using GraphPad PRIZM (ver. 5.01) or the R software package (ver. 3.3.2).

## Results

*Generation of wnt8a mutants by TALENs*

Previous studies of *wnt8a* ORF1 and ORF2 loss by chromosomal deletion or antisense MO-mediated knockdown revealed functions of zygotic *wnt8a* transcripts (Lekven et al., 2001; Shimizu et al., 2005), but did not provide genetic evidence regarding specific

roles for ORF1 and ORF2, or for maternal *wnt8a* transcripts. To address these points, we generated ORF1 and ORF2 single, and ORF1/2 compound mutants by TALENs. We designed TALENs for one target (T1) in ORF1 and two targets (T1, T2) in ORF2 (Fig. 1A, B). We then injected capped RNAs of the ORF1 or ORF2 TALENs alone or combinations of the ORF1 and ORF2 TALENs into one-cell-stage embryos. In subsequent generations, we successfully isolated two ORF1 mutants (*ΔO1-1, 2*), three ORF2 mutants (*ΔO2-1, 2, 3*), three ORF1/ORF2 mutants (*ΔO1ΔO2-1, 2, 3*), and one mutant with a long deletion across the 3' region of ORF1 and the 5' region of ORF2 (*del*) (Fig. 1, Suppl. Fig. 1). All of the mutant alleles except for *del* harbored an indel mutation in the ORF1 and/or the ORF2 that caused a frame shift and introduced a premature stop codon (Fig. 1B, C, D, Suppl. Fig. 1); thus, they were all likely to be null alleles. The data from *ΔO1-1*, *ΔO2-1*, and *ΔO1ΔO2-2* are shown as representative of the ORF1 (*ΔO1*), ORF2 (*ΔO2*), and ORF1/ORF2 compound (*ΔO1ΔO2*) mutants in Fig. 2, 3, 4, and Suppl. Fig. 5. The other ORF1 (*ΔO1-2*), ORF2 (*ΔO2-2, 3*), and ORF1/ORF2 (*ΔO1ΔO2-1, 3*) zygotic mutants showed similar or identical phenotypes to the *ΔO1-1*, *ΔO2-1*, and *ΔO1ΔO2-2* mutants, respectively (Suppl. Fig. 2, 3, 4).

*The ORF1 and ORF2 of wnt8a function redundantly in posterior and ventrolateral tissue formation*

To analyze zygotic homozygous ORF1, ORF2, ORF1/2, and deletion mutants, we crossed their heterozygote pairs (Fig. 2). About a quarter of the embryos from the crosses of the ORF1/2 and deletion mutant pairs showed a lack of yolk extension

(No-YE) at the pharyngula period (30 hpf). In contrast, less than a few percent of the embryos from the crosses of ORF1 or ORF2 single mutants showed the No-YE phenotype (Fig. 2A, Suppl. Fig. 2, Suppl. Table 1). Trans-heterozygotes such as *ΔO1/ΔO1ΔO2* and *ΔO2/ΔO1ΔO2*, which were obtained from the single mutant and compound mutant pairs, scarcely showed the No-YE phenotypes (Suppl. Table 2). Genotyping of the No-YE embryos from the cross of the ORF1/2 or the deletion mutant pairs revealed that all of the No-YE embryos but none of the embryos showing a normal morphology were ORF1/2 homozygotes (Suppl. Fig. 3., Suppl. Table S1). These data indicated that only the embryos lacking both the ORF1 and ORF2 functions displayed the No-YE phenotype, whereas the ORF1 and ORF2 single homozygous mutants and any heterozygous mutants showed no apparent morphological phenotypes at the pharyngula period. The No-YE phenotype is reported to be associated with a reduction or loss of posterior tissues in mutant embryos of *wnt8a* and the *caudal*-related genes *cdx1a*/4 (Hammerschmidt et al., 1996; Lekven et al., 2001; Shimizu et al., 2005). The No-YE embryos showed various degrees of antero-dorsalized phenotypes, so we categorized them into three classes (C1-3) based on the severity of these phenotypes, where C1 was the mildest and C3 was the most severe (Fig. 2B, C). The penetrance and severity of the antero-dorsalized phenotypes were comparable between the ORF1/2 and the deletion mutant alleles (Suppl. Fig. 4).

The expression of *noto* (formerly *floating head*, a marker of axial mesoderm) at the early-gastrula (shield) stage was unaffected in the ORF2 mutants, slightly expanded in the ORF1 mutants, and prominently expanded in the ORF1/2 and deletion

mutants (Fig. 2D, Suppl. Fig. 5). The expression of *tbx6l* (formerly *tbx6*, a paraxial mesodermal marker) at the late gastrula stage (80% epiboly) was not affected in the ORF1 or ORF2 single mutants, but was strongly reduced in the ORF1/2 and deletion mutants (Fig. 2D). The expression of *otx2* (rostral neuroectoderm) at the end of gastrulation (100% epiboly stage) was not affected in the ORF1 or ORF2 single mutants, but was strongly expanded in the ORF1/2 and deletion mutants (Fig. 2D). These data indicated that the ORF1/2 and deletion *wnt8a* mutants showed antero-dorsalized phenotypes: expansion of the axial mesoderm and the rostral neuroectoderm, and reduction of the posterior and ventrolateral tissues. These phenotypes were comparable to the *wnt8a* ORF1/2 morphant and chromosomal deletion mutant embryos (Lekven et al., 2001; Shimizu et al., 2005), further confirming that all of the ORF1/2 and deletion mutants were null alleles of the *wnt8a* gene. These data also demonstrated that both ORF1 and ORF2 are required for the zygotic *wnt8a*-mediated posterior and ventrolateral tissue formation. As the ORF1 mutants displayed a mild dorsalized phenotype (slight expansion of the *noto* expression domain, Suppl. Fig. 5) at the early gastrula stage, *wnt8a* ORF1 may play a more important role than ORF2 at that stage. The loss of ORF1 function was compensated for at a subsequent developmental period in the ORF1 mutants.

*Maternal wnt8a is not essential for the initial dorsal determination*

To reveal the roles of maternal *wnt8a*, we performed germ-line replacement (Ciruna et al., 2002; Saito et al., 2010). We transplanted prospective primordial germ cells, which

were marked by the translation of GFP-Buckyball, from *wnt8a* ORF1/2 (*ΔO1ΔO2-2*) homozygous mutant embryos, into *dead end (dnd1*) morphant embryos, which lack germ cells (Weidinger et al., 2003). The transplant-receiving embryos were reared and treated with estradiol to improve the chance of obtaining female fish with *wnt8a*-deficient germ cells. The transplant-receiving female fish were crossed with wild-type male fish to generate maternal *wnt8a* mutant embryos (M*wnt8a*$^{-/-}$, Fig. 3). Unexpectedly, the M*wnt8a* mutants showed no defects in axis formation at 30 hpf and no apparent morphological phenotypes during development (Fig. 3A). Genotyping of the M*wnt8a* mutant embryos revealed that they were all heterozygotes, with both wild-type and mutant alleles in both ORF1 and ORF2 (Fig. 3B). To exclude the possibility that wild-type *wnt8a* mRNA was transferred from surrounding somatic cells to the oocytes during oogenesis, we performed RT-PCR from one-cell-stage M*wnt8a* mutant embryos. None of them had detectable wild-type *wnt8a* ORF1 or ORF2 transcripts (the data from four embryos are shown in Fig. 3C; four other mutant embryos showed the same results), confirming that the M*wnt8a* mutant embryos lacked wild-type (functional) *wnt8a* mRNA. We also found that the *noto*, *tbx6l*, *otx2*, and *goosecoid* (*gsc*, a dorsal organizer marker at the shield stage) expressions were not affected in the M*wnt8a* mutant embryos (Fig. 3D). These data indicated that maternal *wnt8a* transcripts are dispensable for dorsal axis formation.

*Maternal wnt8a cooperates with zygotic wnt8a in posterior and ventrolateral tissue formation*

As *wnt8a* is expressed both maternally and zygotically (Kelly et al., 1995; Lekven et al., 2001), the maternal *wnt8a* transcripts may cooperate with the zygotic ones. We generated maternal and zygotic *wnt8a* mutants by crossing the female fish with *wnt8a*-deficient germ cells and *wnt8a* heterozygous male fish (the *ΔO1ΔO2-2* allele was used). Approximately half of the embryos showed antero-dorsalized phenotypes, including the No-YE phenotype, at 30 hpf (Fig. 4A, B). This cross was expected to generate M*wnt8a* and MZ*wnt8a* mutants equally, and the MZ*wnt8a* mutants but not the M*wnt8a* mutants showed the antero-dorsalized phenotypes. The expression of *noto*, *tbx6l*, and *otx2* was laterally expanded, reduced, and posteriorly expanded, respectively, in the MZ*wnt8a* mutant embryos (Fig. 4C), as seen in the zygotic (Z) *wnt8a* mutants (Fig. 2D). Although the aberrant expression of these markers was not obviously different between the Z*wnt8a* and MZ*wnt8a* mutants, the severity of the antero-dorsalized phenotypes was significantly different (chi-square test, $P < 0.001$, compare Fig. 2C and Fig. 4B). More MZ*wnt8a* mutants showed the severe phenotype C3, than Z*wnt8a* mutants.

During our experiments, we obtained a *ΔO1ΔO2-3* homozygous adult female fish, which showed no obvious abnormal phenotypes, for unknown reasons. We obtained embryos by crossing this homozygous female and a heterozygous *ΔO1ΔO2-3* mutant fish. Approximately half of the embryos showed the No-YE phenotype, whereas the other half showed a normal morphology, suggesting that the No-YE embryos were MZ*wnt8a* mutants (Suppl. Fig. 6A). We then compared the antero-dorsalized phenotypes of the Z*wnt8a*$^{\Delta O1\Delta O2\text{-}3}$ and MZ*wnt8a*$^{\Delta O1\Delta O2\text{-}3}$ mutants. As observed in the

*wnt8a*$^{\Delta O1\Delta O2\text{-}2}$ mutants, more MZ*wnt8a* mutants showed more severe phenotypes (the severity was significantly different between the Z and MZ*wnt8a*$^{\Delta O1\Delta O2\text{-}3}$ mutant embryos, chi-square test, $P < 0.001$, Suppl. Fig. 6B).

These data indicated that a loss of maternal *wnt8a* transcript enhanced the antero-dorsalized phenotypes in zygotic *wnt8a*-deficient embryos, suggesting that the maternal *wnt8a* transcripts cooperated with zygotic *wnt8a* transcripts in posterior and ventrolateral tissue formation.

*Maternal wnt6a is an alternative DD candidate*

Since maternal *wnt8a* was not essential for dorsal axis formation, we considered two possibilities. First, other *wnt* genes could be upregulated in the M*wnt8a* mutant oocytes to compensate for the *wnt8a* deficiency, since deleterious mutations generated by genome-editing systems such as TALENs are reported to induce genetic compensation (Rossi et al., 2015). Alternatively, other *wnt* gene(s) that are maternally deposited could induce the canonical Wnt pathway for the initial dorsal determination, i.e., function as DDs. With these possibilities in mind, we re-searched the databases and found that *wnt6a* and *wnt7ab* were additionally identified after the original publication (Lu et al., 2011) that proposed *wnt8a* as a DD candidate (*wnt6* and *wnt7a* were renamed *wnt6b* and *wnt7aa*, respectively, in ZFIN). We then re-examined the maternal expression of the *wnt* genes in oocytes from wild-type and from the female fish with *wnt8a*-deficient germ cells (*wnt8a*-deficient oocytes) by semi-quantitative RT-PCR. None of the *wnt* gene expressions were upregulated in the M*wnt8a*-deficient compared to wild-type oocytes

(Fig. 5), suggesting that genetic compensation did not take place, at least in the *wnt* gene loci examined.

We also found that among the *wnt* genes, *wnt6a* and *wnt8a* were more strongly expressed in oocytes than in pharyngula-stage embryos (Fig. 5). We therefore examined expression of *wnt6a* and *wnt7ab* in one-cell-stage embryos by whole-mount *in situ* hybridization. Although *wnt7ab* was not detected, *wnt6a* transcripts were detected in the vegetal pole of the yolk in a portion of the embryos examined, similar to *wnt8a* (Fig. 6A), suggesting that maternal *wnt6a* is a potential DD candidate. To investigate the activity of Wnt6a, we injected capped and polyadenylated RNAs for *wnt6a*, *wnt8a*, and/or *dkk1b*, which encodes a Wnt inhibitor that potentially blocks the canonical Wnt pathway at the receptor level (Glinka et al., 1998; Mao et al., 2002; Mao et al., 2001), into one-cell-stage embryos. The overexpression of Wnt6a led to embryonic posteriorization (no eyes) and mild dorsalization (curled tail), similar to the overexpression of Wnt8a (Fig. 6B), suggesting that Wnt6a can induce the canonical Wnt pathway that is involved in posteriorization. The co-expression of Dkk1b antagonized Wnt8a's activity and reversed the phenotype (anteriorization) (Fig. 6B). The co-expression of Dkk1b also reversed and anteriorized the *wnt6a* RNA-injected embryos (Fig. 6B). The injection of *wnt6a* or *wnt8a* RNA led to an expanded or ectopic expression of *dharma*, a target of the canonical Wnt pathway that is involved in dorsal organizer formation (Fekany et al., 1999; Koos and Ho, 1999; Leung et al., 2003; Ryu et al., 2001; Shimizu et al., 2002; Yamanaka et al., 1998) in a large proportion of the embryos (Fig. 6C). In agreement with this finding, the overexpression of Dkk1b

inhibited the *dharma* expression, similar to the overexpression of ΔN-Tcf7l1a (formerlyΔN-Tcf3a). These data suggested that Wnt ligand(s) are involved in the initial dorsal determination in zebrafish embryos, and that maternal Wnt6a is a candidate Wnt ligand DDs that induces the dorsal axis.

## Discussion

*Roles of zygotic wnt8a in posterior and ventrolateral tissue formation*

The ORF1 and ORF2 of *wnt8a* encode two related Wnt8a proteins that have approximately 70% amino acid identity (Lekven et al., 2001). Multiple *wnt8a* transcripts that include ORF1-ORF2 (potentially bicistronic) and ORF2-specific transcripts are transcribed in gastrula embryos, using multiple enhancer/promoter elements and transcriptional start sites (Lekven et al., 2001; Narayanan and Lekven, 2012). *In situ* hybridization with ORF1/2-specific probes revealed that the ORF1 and ORF2 transcripts are co-expressed in the non-axial mesoderm, and that the ORF2 transcript is expressed in additional domains, including portions of the axial mesoderm and hindbrain (Lekven et al., 2001), suggesting that each ORF has some specific roles in development. However, antisense MO-mediated knockdown of ORF1 or ORF2 alone does not elicit significant effects on embryonic patterning, whereas the knockdown of both ORF1 and ORF2 results in antero-dorsalization, as seen in chromosomal deletion mutants lacking the *wnt8a* gene (Lekven et al., 2001; Shimizu et al., 2005). The side effects of antisense MOs have been debated (Stainier et al., 2015), and chromosomal

deletion mutants may lack additional gene(s) (Lekven et al., 2001). In contrast, analyses using the ORF1, ORF2, ORF1/2, and deletion mutants established in this study (Fig. 1, Suppl. Fig. 1) should provide definitive genetic evidence for specific and redundant roles of *wnt8a* ORF1 and ORF2.

The zygotic ORF1 mutants displayed a weak expansion of *noto* expression in the axial mesoderm at the early-gastrula period, but did not show an apparent phenotype at the pharyngula period (Fig. 2, Suppl. Fig. 5). The zygotic ORF2 mutants showed no abnormalities in marker expression at the gastrula period or in embryonic morphology at the pharyngula period (Fig. 2). Only the zygotic ORF1/2 homozygote mutants showed antero-dorsalized phenotypes at the pharyngula period (Fig. 2). These data suggested that although *wnt8a* ORF1 plays a major role in restricting the dorsal mesoderm region at the early and mid-gastrula stage, *wnt8a* ORF2 can compensate for the loss of ORF1 function at later developmental stages. While it is not clear whether the Wnt8a ORF1 and ORF2 proteins are translated from the same transcript (ORF1-ORF2) or separate transcripts (e.g. ORF1-ORF2 and ORF2-specific), the Wnt8a ORF1 and the ORF2 proteins function redundantly in posterior and the ventrolateral tissue formation. Although we did not find any obvious phenotypes in the ORF2 mutants in this study, ORF2-specific expression domains are reported (Lekven et al., 2001). Therefore, future studies with the ORF2 single mutants may reveal ORF2-specific roles of Wnt8a in development.

*Roles of maternal wnt8a in dorsal-axis formation*

Maternal *wnt8a* mutants showed no defects in dorsal axis formation (Fig. 3), indicating that the maternal *wnt8a* transcripts are dispensable for this axis formation. It is possible that wild-type *wnt8a* mRNA or Wnt8a protein was transferred from the surrounding somatic cells to the oocytes in the wild-type female fish with *wnt8a*-deficient germ cells. However, the M*wnt8a* mutant embryos contained only the mutant forms of *wnt8a* ORF1 and ORF2 transcripts (Fig. 3). The M*wnt8a* mutant embryos from the *wnt8a* ORF1/2 (*ΔO1ΔO2-3*) homozygous female fish, which lacked wild-type ORF1 and ORF2 in both germ and somatic cells (Suppl. Fig S1), also showed no defects in dorsal axis formation (Suppl. Fig. 6). Our data indicated that the M*wnt8a* mutant embryos analyzed in this study completely lacked functional Wnt8a ORF1 and ORF2 proteins. It was recently reported that indel mutations generated by TALENs can induce genetic compensation (Rossi et al., 2015). Thus, it is possible that the maternal expression of other *wnt* gene(s) was upregulated in the M*wnt8a* mutant oocytes (and embryos) and compensated for the loss of maternal *wnt8a* transcripts. However, we detected no upregulated expression of known *wnt* genes in the M*wnt8a* mutant oocytes (Fig. 5). These data suggested that the genomic compensation by other *wnt* genes was not responsible for the normal axis formation in the M*wnt8a* mutants, although we cannot exclude the possibility that genes other than *wnt* genes compensated for the *wnt8a* deficiency.

The 3' untranslated region (3' UTR) of maternal *nodal-related 1* (known as *squint*) transcripts is known to function upstream of the canonical Wnt pathway in an ORF-independent manner (Lim et al., 2012). As our mutant alleles retained the 3'UTR of *wnt8a* ORF2, the 3'UTR of *wnt8a* mRNAs may also function in dorsal axis

formation in an ORF-independent manner. Although such a possibility remains elusive, our data clearly indicated that maternal Wnt8a proteins translated from maternal *wnt8a* transcripts are dispensable for the dorsal axis formation.

On the other hand, we found that maternal *wnt8a* transcripts play a role at a later developmental stage. Although the M*wnt8a* mutants displayed no apparent phenotypes, the MZ*wnt8a* mutants showed more severe antero-dorsalized phenotypes than the Z*wnt8a* mutant embryos (Fig. 4, Suppl. Fig 6), suggesting that maternal *wnt8a* transcripts are involved in posterior and ventrolateral tissue formation. During gastrulation, many *wnt* genes that activate canonical Wnt signaling, including *wnt8a* and *wnt3a*, are expressed (Lekven et al., 2001; Lu et al., 2011; Shimizu et al., 2005). A gradual reduction in Wnt molecules by antisense *wnt8a* and/or *wnt3a* MOs leads to a progressive reduction of the posterior structures (Shimizu et al., 2005), suggesting that the total amount of Wnt ligands for canonical signaling in the gastrula embryo is critical for precise embryonic patterning. The MZ*wnt8a* mutant embryos might have lower amounts of canonical Wnt ligands at the gastrula period than do the Z*wnt8a* mutant embryos, resulting in more severe phenotypes. Thus, it is possible that Wnt8a proteins from maternal transcripts cooperate with Wnt8a proteins from zygotic transcripts in posterior and ventrolateral tissue formation.

*Are Wnts involved in the initial dorsal determination?*

The lack of axis defects in the M*wnt8a* mutants (Fig. 3) raised the questions of whether maternal *wnt8a* transcripts play any role in dorsal axis formation and whether Wnt

ligands are required for the initial dorsal determination. The expression of dominant-negative Tcf71la (Tcf3a), or the overexpression of Axin, Axin2, and/or Gsk3ab, all of which inhibit Wnt cytoplasmic signaling, was reported to reduce or abrogate the expression of dorsal-specific genes (Ryu et al., 2001; Shimizu et al., 2000) (Fig. 6). The *ichabod* mutants, which have reduced maternal β-catenin2 expression, display defects in dorsal axis formation (Bellipanni et al., 2006; Kelly et al., 2000). These reports suggest that cytoplasmic Wnt signaling to the β-catenin/Tcf complex plays an essential role in dorsal axis formation. However, the overexpression of Dkk1 (Dkk1b in zebrafish), which inhibits the canonical Wnt pathway at the level of the Wnt receptor LRP6 (Mao et al., 2002; Mao et al., 2001), in early-stage *Xenopus* and zebrafish embryos did not lead to ventralization of the embryos or inhibit the expression of dorsal-specific genes (Glinka et al., 1998; Hashimoto et al., 2000; Shinya et al., 2000), suggesting that Wnt ligands that activate canonical signaling (canonical Wnt ligands) are dispensable for dorsal axis formation. In this study, we injected a large amount of capped and polyadenylated *dkk1b* RNA (Fig. 6), which might be translated to the protein more efficiently than that used in the previous study (Hashimoto et al., 2000). The overexpression of Dkk1b inhibited the *dharma* expression in about half of the injected embryos, suggesting that canonical Wnt ligands do have a role in dorsal axis formation. This result is consistent with the previous finding that expressing dominant-negative Wnt8a or secreted Wnt antagonist Frzb, which may inhibit canonical Wnt ligands other than Wnt8a, strongly reduces or abrogates the *chordin* expression (Lu et al., 2011). There are possible explanations for the incomplete inhibition of *dharma*

and the dorsal axis formation by Dkk1b. It may be due to an insufficient translation of Dkk1b to overcome the Wnt ligand(s) acting on the receptor complex in the initial dorsalization. Alternatively, the early (maternal) and late (zygotic) Wnt pathways exhibit opposite functions in axis formation. Thus, although Dkk1b might inhibit the maternal canonical Wnt pathway and dorsal axis formation, Dkk1b could also rescue ventralized phenotypes, by blocking the zygotic Wnt pathway, leading to dorsalization. In any case, canonical Wnt ligands are likely involved in the initial dorsal determination. We found that *wnt6a* transcripts were maternally deposited to the vegetal pole of the yolk and Wnt6a was more potent for posteriorizing the embryos (indicative of zygotic canonical Wnt signaling) than Wnt8a (Fig. 6). Collectively, our data suggested that maternal Wnt6a is an alternative DD candidate. Although M*wnt8a* mutants showed no defects in dorsal determination, maternal *wnt6a* transcripts could have compensated for the maternal *wnt8a* deficiency. In this sense, Wnt8a, Wnt6a, and possibly other Wnts that are expressed maternally (Fig. 5) may cooperate to activate the canonical Wnt pathway to induce the dorsal-specific genes that are required for dorsal axis formation. Future studies with zebrafish mutants lacking the maternal transcripts of multiple *wnt* genes, and visualization of the Wnt proteins should shed light on the identification of the DDs and mechanisms of dorsal axis formation.

**Acknowledgements**

We thank R. Moon, H. Hashimoto, R.I. Dorsky, and K. Inoue for the expression

plasmids for *wnt8a*, *dkk1b*, *ΔN-tcf7l1a*, and *GFP-buc*, respectively, T. Yamamoto and K. Hoshijima for the TALEN-related plasmids, B. Ciruna for technical advice for germ-line replacement, Y. Tsukazaki and K. Kondoh for fish mating and care, and the members of the Hibi laboratory for helpful discussion. This work was supported by JSPS KAKENHI Grant Number JP21370103 and JP 24657152 (to M.H.).

**References**

Bellipanni, G., Varga, M., Maegawa, S., Imai, Y., Kelly, C., Myers, A.P., Chu, F., Talbot, W.S., Weinberg, E.S., 2006. Essential and opposing roles of zebrafish beta-catenins in the formation of dorsal axial structures and neurectoderm. Development 133, 1299-1309.

Cai, Q., Gerwin, C., Sheng, Z.H., 2005. Syntabulin-mediated anterograde transport of mitochondria along neuronal processes. J Cell Biol 170, 959-969.

Cai, Q., Pan, P.Y., Sheng, Z.H., 2007. Syntabulin-kinesin-1 family member 5B-mediated axonal transport contributes to activity-dependent presynaptic assembly. J Neurosci 27, 7284-7296.

Cermak, T., Doyle, E.L., Christian, M., Wang, L., Zhang, Y., Schmidt, C., Baller, J.A., Somia, N.V., Bogdanove, A.J., Voytas, D.F., 2011. Efficient design and assembly of custom TALEN and other TAL effector-based constructs for DNA targeting. Nucleic acids research 39, e82.

Cha, S.W., Tadjuidje, E., Tao, Q., Wylie, C., Heasman, J., 2008. Wnt5a and Wnt11 interact in a maternal Dkk1-regulated fashion to activate both canonical and non-canonical signaling in Xenopus axis formation. Development 135, 3719-3729.

Cha, S.W., Tadjuidje, E., White, J., Wells, J., Mayhew, C., Wylie, C., Heasman, J., 2009. Wnt11/5a complex formation caused by tyrosine sulfation increases canonical signaling activity. Curr Biol 19, 1573-1580.

Ciruna, B., Weidinger, G., Knaut, H., Thisse, B., Thisse, C., Raz, E., Schier, A.F., 2002. Production of maternal-zygotic mutant zebrafish by germ-line replacement. Proc Natl

Acad Sci U S A 99, 14919-14924.
Dahlem, T.J., Hoshijima, K., Jurynec, M.J., Gunther, D., Starker, C.G., Locke, A.S., Weis, A.M., Voytas, D.F., Grunwald, D.J., 2012. Simple methods for generating and detecting locus-specific mutations induced with TALENs in the zebrafish genome. PLoS genetics 8, e1002861.
Dorsky, R.I., Itoh, M., Moon, R.T., Chitnis, A., 2003. Two tcf3 genes cooperate to pattern the zebrafish brain. Development 130, 1937-1947.
Dougan, S.T., Warga, R.M., Kane, D.A., Schier, A.F., Talbot, W.S., 2003. The role of the zebrafish nodal-related genes squint and cyclops in patterning of mesendoderm. Development 130, 1837-1851.
Fekany, K., Yamanaka, Y., Leung, T., Sirotkin, H.I., Topczewski, J., Gates, M.A., Hibi, M., Renucci, A., Stemple, D., Radbill, A., Schier, A.F., Driever, W., Hirano, T., Talbot, W.S., Solnica-Krezel, L., 1999. The zebrafish bozozok locus encodes Dharma, a homeodomain protein essential for induction of gastrula organizer and dorsoanterior embryonic structures. Development 126, 1427-1438.
Ge, X., Grotjahn, D., Welch, E., Lyman-Gingerich, J., Holguin, C., Dimitrova, E., Abrams, E.W., Gupta, T., Marlow, F.L., Yabe, T., Adler, A., Mullins, M.C., Pelegri, F., 2014. Hecate/Grip2a acts to reorganize the cytoskeleton in the symmetry-breaking event of embryonic axis induction. PLoS genetics 10, e1004422.
Glinka, A., Wu, W., Delius, H., Monaghan, A.P., Blumenstock, C., Niehrs, C., 1998. Dickkopf-1 is a member of a new family of secreted proteins and functions in head induction. Nature 391, 357-362.
Hammerschmidt, M., Pelegri, F., Mullins, M.C., Kane, D.A., Brand, M., van Eeden, F.J., Furutani-Seiki, M., Granato, M., Haffter, P., Heisenberg, C.P., Jiang, Y.J., Kelsh, R.N., Odenthal, J., Warga, R.M., Nusslein-Volhard, C., 1996. Mutations affecting morphogenesis during gastrulation and tail formation in the zebrafish, Danio rerio. Development 123, 143-151.
Hashimoto, H., Itoh, M., Yamanaka, Y., Yamashita, S., Shimizu, T., Solnica-Krezel, L., Hibi, M., Hirano, T., 2000. Zebrafish Dkk1 functions in forebrain specification and axial mesendoderm formation. Dev Biol 217, 138-152.
Hibi, M., Hirano, T., Dawid, I.B., 2002. Organizer formation and function. Results Probl Cell Differ 40, 48-71.
Jesuthasan, S., Stahle, U., 1997. Dynamic microtubules and specification of the

zebrafish embryonic axis. Curr Biol 7, 31-42.
Kelly, C., Chin, A.J., Leatherman, J.L., Kozlowski, D.J., Weinberg, E.S., 2000. Maternally controlled (beta)-catenin-mediated signaling is required for organizer formation in the zebrafish. Development 127, 3899-3911.
Kelly, G.M., Greenstein, P., Erezyilmaz, D.F., Moon, R.T., 1995. Zebrafish wnt8 and wnt8b share a common activity but are involved in distinct developmental pathways. Development 121, 1787-1799.
Kimmel, C.B., Ballard, W.W., Kimmel, S.R., Ullmann, B., Schilling, T.F., 1995. Stages of embryonic development of the zebrafish. Dev Dyn 203, 253-310.
Koos, D.S., Ho, R.K., 1999. The nieuwkoid/dharma homeobox gene is essential for bmp2b repression in the zebrafish pregastrula. Dev Biol 215, 190-207.
Langdon, Y.G., Mullins, M.C., 2011. Maternal and zygotic control of zebrafish dorsoventral axial patterning. Annu Rev Genet 45, 357-377.
Lekven, A.C., Thorpe, C.J., Waxman, J.S., Moon, R.T., 2001. Zebrafish wnt8 encodes two wnt8 proteins on a bicistronic transcript and is required for mesoderm and neurectoderm patterning. Dev Cell 1, 103-114.
Leung, T., Bischof, J., Soll, I., Niessing, D., Zhang, D., Ma, J., Jackle, H., Driever, W., 2003. bozozok directly represses bmp2b transcription and mediates the earliest dorsoventral asymmetry of bmp2b expression in zebrafish. Development 130, 3639-3649.
Lim, S., Kumari, P., Gilligan, P., Quach, H.N., Mathavan, S., Sampath, K., 2012. Dorsal activity of maternal squint is mediated by a non-coding function of the RNA. Development 139, 2903-2915.
Lu, F.I., Thisse, C., Thisse, B., 2011. Identification and mechanism of regulation of the zebrafish dorsal determinant. Proc Natl Acad Sci U S A 108, 15876-15880.
Mao, B., Wu, W., Davidson, G., Marhold, J., Li, M., Mechler, B.M., Delius, H., Hoppe, D., Stannek, P., Walter, C., Glinka, A., Niehrs, C., 2002. Kremen proteins are Dickkopf receptors that regulate Wnt/beta-catenin signalling. Nature 417, 664-667.
Mao, B., Wu, W., Li, Y., Hoppe, D., Stannek, P., Glinka, A., Niehrs, C., 2001. LDL-receptor-related protein 6 is a receptor for Dickkopf proteins. Nature 411, 321-325.
Mizuno, T., Yamaha, E., Kuroiwa, A., Takeda, H., 1999. Removal of vegetal yolk causes dorsal deficencies and impairs dorsal-inducing ability of the yolk cell in zebrafish.

Mech Dev 81, 51-63.
Narayanan, A., Lekven, A.C., 2012. Biphasic wnt8a expression is achieved through interactions of multiple regulatory inputs. Dev Dyn 241, 1062-1075.
Nojima, H., Rothhamel, S., Shimizu, T., Kim, C.H., Yonemura, S., Marlow, F.L., Hibi, M., 2010. Syntabulin, a motor protein linker, controls dorsal determination. Development 137, 923-933.
Nojima, H., Shimizu, T., Kim, C.H., Yabe, T., Bae, Y.K., Muraoka, O., Hirata, T., Chitnis, A., Hirano, T., Hibi, M., 2004. Genetic evidence for involvement of maternally derived Wnt canonical signaling in dorsal determination in zebrafish. Mech Dev 121, 371-386.
Ober, E.A., Schulte-Merker, S., 1999. Signals from the yolk cell induce mesoderm, neuroectoderm, the trunk organizer, and the notochord in zebrafish. Dev Biol 215, 167-181.
Ota, S., Hisano, Y., Muraki, M., Hoshijima, K., Dahlem, T.J., Grunwald, D.J., Okada, Y., Kawahara, A., 2013. Efficient identification of TALEN-mediated genome modifications using heteroduplex mobility assays. Genes to cells : devoted to molecular & cellular mechanisms 18, 450-458.
Rossi, A., Kontarakis, Z., Gerri, C., Nolte, H., Holper, S., Kruger, M., Stainier, D.Y., 2015. Genetic compensation induced by deleterious mutations but not gene knockdowns. Nature 524, 230-233.
Ryu, S.L., Fujii, R., Yamanaka, Y., Shimizu, T., Yabe, T., Hirata, T., Hibi, M., Hirano, T., 2001. Regulation of dharma/bozozok by the Wnt pathway. Dev Biol 231, 397-409.
Saito, T., Goto-Kazeto, R., Arai, K., Yamaha, E., 2008. Xenogenesis in teleost fish through generation of germ-line chimeras by single primordial germ cell transplantation. Biol Reprod 78, 159-166.
Saito, T., Goto-Kazeto, R., Fujimoto, T., Kawakami, Y., Arai, K., Yamaha, E., 2010. Inter-species transplantation and migration of primordial germ cells in cyprinid fish. Int J Dev Biol 54, 1481-1486.
Saito, T., Psenicka, M., Goto, R., Adachi, S., Inoue, K., Arai, K., Yamaha, E., 2014. The origin and migration of primordial germ cells in sturgeons. PloS one 9, e86861.
Sakuma, T., Hosoi, S., Woltjen, K., Suzuki, K., Kashiwagi, K., Wada, H., Ochiai, H., Miyamoto, T., Kawai, N., Sasakura, Y., Matsuura, S., Okada, Y., Kawahara, A., Hayashi, S., Yamamoto, T., 2013. Efficient TALEN construction and evaluation methods for

human cell and animal applications. Genes to cells : devoted to molecular & cellular mechanisms 18, 315-326.
Schier, A.F., Talbot, W.S., 2005. Molecular genetics of axis formation in zebrafish. Annu Rev Genet 39, 561-613.
Schneider, S., Steinbeisser, H., Warga, R.M., Hausen, P., 1996. Beta-catenin translocation into nuclei demarcates the dorsalizing centers in frog and fish embryos. Mech Dev 57, 191-198.
Shimizu, T., Bae, Y.K., Muraoka, O., Hibi, M., 2005. Interaction of Wnt and caudal-related genes in zebrafish posterior body formation. Dev Biol 279, 125-141.
Shimizu, T., Yamanaka, Y., Nojima, H., Yabe, T., Hibi, M., Hirano, T., 2002. A novel repressor-type homeobox gene, ved, is involved in dharma/bozozok-mediated dorsal organizer formation in zebrafish. Mech Dev 118, 125-138.
Shimizu, T., Yamanaka, Y., Ryu, S., Hashimoto, H., Yabe, T., Hirata, T., Bae, Y., Hibi, M., Hirano, T., 2000. Cooperative roles of Bozozok/Dharma and nodal-related proteins in the formation of the dorsal organizer in zebrafish. Mech Dev 91, 293-303.
Shinya, M., Eschbach, C., Clark, M., Lehrach, H., Furutani-Seiki, M., 2000. Zebrafish Dkk1, induced by the pre-MBT Wnt signaling, is secreted from the prechordal plate and patterns the anterior neural plate. Mech Dev 98, 3-17.
Stainier, D.Y., Kontarakis, Z., Rossi, A., 2015. Making sense of anti-sense data. Dev Cell 32, 7-8.
Su, Q., Cai, Q., Gerwin, C., Smith, C.L., Sheng, Z.H., 2004. Syntabulin is a microtubule-associated protein implicated in syntaxin transport in neurons. Nat Cell Biol 6, 941-953.
Tao, Q., Yokota, C., Puck, H., Kofron, M., Birsoy, B., Yan, D., Asashima, M., Wylie, C.C., Lin, X., Heasman, J., 2005. Maternal wnt11 activates the canonical wnt signaling pathway required for axis formation in Xenopus embryos. Cell 120, 857-871.
Thisse, C., Thisse, B., 1998. High Resolution Whole-Mount in situ Hybridization, Zebrafish Science Monitor.
Tran, L.D., Hino, H., Quach, H., Lim, S., Shindo, A., Mimori-Kiyosue, Y., Mione, M., Ueno, N., Winkler, C., Hibi, M., Sampath, K., 2012. Dynamic microtubules at the vegetal cortex predict the embryonic axis in zebrafish. Development 139, 3644-3652.
Weidinger, G., Stebler, J., Slanchev, K., Dumstrei, K., Wise, C., Lovell-Badge, R., Thisse, C., Thisse, B., Raz, E., 2003. dead end, a novel vertebrate germ plasm

component, is required for zebrafish primordial germ cell migration and survival. Curr Biol 13, 1429-1434.
Westerfield, M., 1995. The Zebrafish Book: A Guide for the Laboratory Use of Zebrafish. University of Oregon Press, Eugene, OR.
Yamanaka, Y., Mizuno, T., Sasai, Y., Kishi, M., Takeda, H., Kim, C.H., Hibi, M., Hirano, T., 1998. A novel homeobox gene, dharma, can induce the organizer in a non-cell-autonomous manner. Genes Dev 12, 2345-2353.

**Figure legends**

**Fig. 1** Generation of *wnt8a* mutants.

(A) Schematic of the *wnt8a* gene structure in zebrafish (to scale). Two ORFs (ORF1, ORF2) are tandemly located and encode two Wnt8a proteins. The 5' and 3' non-coding exons are indicated by black boxes, and ORF1 and ORF2 by green and orange boxes, respectively. The positions of the translational initiation sites and stop codons are indicated. The position of the target regions of the TALENs is indicated by bars with T1 and T2. (B, C) *wnt8a*$_{\Delta O1}$, *wnt8a*$_{\Delta O2}$, *wnt8a*$_{\Delta O1\Delta O2}$, and *wnt8a*$_{del}$ mutants generated by TALENs. One and two sets of TALENs were generated and used to introduce mutations in ORF1 (T1) and ORF2 (T1 and T2), respectively. Two and three mutants had an indel mutation in ORF1 (*ΔO1-1,2*) or ORF2 (*ΔO2-1,2,3*), respectively; three mutants had indel mutations in both ORF1 and ORF2 (*ΔO1ΔO2-1,2,3*); and one mutant had a long deletion in the ORF1/ORF2 region (*del*). Partial sequences of the *wnt8a* ORF1 and ORF2 genes in wild-type (WT) and a typical mutant from each group (*ΔO1-1, ΔO2-1, ΔO1ΔO2-2*, and *del*) are shown in (B). These mutants were used for the analyses shown in Fig. 2, 3, 4, and Suppl. Fig. 5. The sequence information of all of the *wnt8a* mutants is shown in Suppl. Fig. 1. The binding sites of the TALENs are indicated by boxes with T1-L/R or T2-L/R (B). The putative protein structures from the WT and mutant genes (*ΔO1*, *ΔO2*, *ΔO1ΔO2*, and *del*) are shown in (C). Gray boxes indicate an insertion of non-relevant amino acids. (D) Detection of the mutant alleles by genomic PCR. The PCR products were separated by acrylamide gel electrophoresis. The positions of a

100-bp marker (M) are indicated. The mutant PCR products are indicated by asterisks. Although a band was seen at the position of the wild-type ORF1 PCR product in the *ΔO1* homozygous mutant, it was non-specific, since it was also detected in the *del* mutants. For the *wnt8a*$_{del}$ allele, PCR primers detecting the WT (upper panel) and the deletion allele (lower panel) were designed separately.

**Fig. 2** Role of ORF1 and ORF2 in the zygotic *wnt8a*-mediated development of caudal and ventrolateral tissues.

(A) Percentage of mutants showing a lack of yolk extension (no yolk extension: No-YE). Embryos were obtained by crossing WT, or *wnt8a*$_{\Delta O1}$(*ΔO1*), *wnt8a*$_{\Delta O2}$ (*ΔO2*), *wnt8a*$_{\Delta O1\Delta O2}$ (*ΔO1ΔO2*), or *wnt8a*$_{del}$ (*del*) heterozygote pairs. Phenotypes were observed at 30 hpf. The number of observed embryos is indicated. (B) WT and *wnt8a* mutant phenotypes. Lateral views with anterior to the left. The No-YE embryos were categorized into three classes. C1 embryos had a slightly shortened and ventrally bent tail, C2 embryos had a short and curled tail, and C3 embryos had an enlarged head and a truncated tail. This phenotype classification is essentially the same as one described in a previous publication (Shimizu et al., 2005), except for being based on the No-YE phenotype. (C) Proportion of No-YE embryos showing each phenotype class. The number of observed embryos is indicated. (D) Expression of *noto* (formerly called *floating head*, shield stage, a-e), *tbx6l* (*tbx6*, 80% epiboly stage, f-j), and *otx2* (100% epiboly stage, k-o) in WT (a, f, k) and *ΔO1* (b, g, l), *ΔO2* (c, h, m), *ΔO1ΔO2* (d, i, n), and *del* (e, j, o) homozygous mutants. Animal pole views with dorsal to the right (a-e).

Lateral views with dorsal to the right (f-o). *noto*, *tbx6l*, and *otx2* are markers of the axial mesoderm, the paraxial mesoderm, and the rostral neuroectoderm (forebrain and midbrain), respectively. The lateral limits of *noto* expression are marked by arrows, the rostral and caudal limits of *otx2* expression are marked by arrowheads, and the ventral limit of *otx2* expression is marked by an asterisk. The *noto* expression was not greatly affected in the *ΔO1* and *ΔO2* single mutants, but it was prominently expanded in the *ΔO1ΔO2* and *del* mutants (*ΔO1*, n=0/86; *ΔO2*, n=0/94; *ΔO1ΔO2*, n=10/42; *del*, n=15/44 in embryos from the heterozygous crosses; *ΔO1*, n=0/7; *ΔO2*, n=0/7; *ΔO1ΔO2*, n=4/4; *del*, n=6/6 in genotyped homozygotes). The *tbx6l* expression was not affected in the *ΔO1* or *ΔO2* mutants, but was reduced or absent in the *ΔO1ΔO2* and *del* mutants (*ΔO1*, n=0/353; *ΔO2*, n=0/96; *ΔO1ΔO2*, n=27/83; *del*, n=37/140 in embryos from the heterozygous crosses; *ΔO1*, n=0/22; *ΔO2*, n=0/9; *ΔO1ΔO2*, n=11/11; *del*, n=10/10 in the genotyped homozygotes). The *otx2* expression was not affected in the *ΔO1* or *ΔO2* mutants, but was expanded in the *ΔO1ΔO2* and *del* mutants (*ΔO1*, n=0/73; *ΔO2*, n=0/99; *ΔO1ΔO2*, n=10/49; *del*, n=18/57 in embryos from the heterozygous crosses; *ΔO1*, n=0/6; *ΔO2*, n=0/7; *ΔO1ΔO2*, n=6/6; *del*, n=6/6 in genotyped homozygotes). Scale bars: 500 μm in B; 200 μm in D.

**Fig. 3** Maternal *wnt8a* mutants show no defects in dorsal-axis formation.

(A) Maternal *wnt8a* mutant embryos (M*wnt8a*$^{-/-}$) at 30 dpf. Embryos were obtained by crossing WT male fish and female fish with *wnt8a*$^{ΔO1ΔO2/ΔO1ΔO2}$ germ cells. Lateral view with anterior to the left. The M*wnt8a*$^{-/-}$ mutant embryos showed no apparent

abnormality in dorsal axis formation (*n*=190). (B, C) Genotyping and RT-PCR of M*wnt8* mutant embryos. The TALEN target regions of ORF1 (upper panel) and ORF2 (lower panel) were amplified by PCR from the genome of a WT and eight M*wnt8a* mutant embryos (B), and by RT-PCR from the RNA of a one-cell-stage WT and four M*wnt8a* mutant embryos (C). The PCR products were separated on acrylamide gels. The positions of the PCR bands corresponding to the mutant DNAs are marked by asterisks. "+" and "-" indicate the presence and absence of reverse transcriptase (RT) in the cDNA synthesis. Note that all of the M*wnt8a* mutant embryos had both WT and mutant alleles (*n*=8/8), and all four M*wnt8a* mutants had only mutant ORF1 and ORF2 transcripts. (D) Expression of *noto* (shield stage, a, b), *tbx6l* (80% epiboly stage, c, d), *otx2* (100% epiboly stage, e, f), and *gsc* (shield stage, g, h) in WT and M*wnt8a* mutants. M*wnt8a* mutants were obtained by crossing female fish with *wnt8a*$^{\Delta O1\Delta O2/\Delta O1\Delta O2}$ germ cells and WT (b, d, f) or *wnt8a*$^{\Delta O1\Delta O2/+}$ male (h) fish. Animal pole views with dorsal to the right (a, b, g, h). Lateral views with dorsal to the right (c-f). The expression of *noto*, *tbx6l*, *otx2*, and *gsc* was unaffected in the M*wnt8a* mutants compared to WT embryos (*noto*, n=20; *tbx6l*, n=20; *otx2*, n=20; *gsc*, n=16). Scale bars: 500 μm in A; 200 μm in D.

**Fig. 4** Maternal *wnt8a* supports the functions of zygotic *wnt8a*.

(A) Phenotype of maternal-zygotic *wnt8a* mutant (MZ*wnt8a*$^{-/-}$) embryos at 30 hpf. Embryos were obtained by crossing *wnt8a*$^{\Delta O1\Delta O2/+}$ male fish and female fish with *wnt8a*$^{\Delta O1\Delta O2/\Delta O1\Delta O2}$ germ cells. Lateral view with anterior to the left. Approximately half of the embryos were predicted to be MZ*wnt8a*$^{-/-}$ embryos, and the rest were M*wnt8a*$^{-/-}$

embryos. The MZ*wnt8a*$^{-/-}$ embryos were identified by genotyping. (B) Percentage of embryos showing the no-yolk extension phenotype (No-YE, left panel), and of No-YE embryos showing the antero-dorsalized phenotypes C1-3 (right panel, Fig. 2B). MZ*wnt8a* showed more severe antero-dorsalized phenotypes than did zygotic (Z) *wnt8a* mutants (*ΔO1ΔO2* in Fig. 2C). The proportions of C1-3 embryos were significantly different between the Z*wnt8a* and MZ*wnt8a* mutants (chi-square test, $P < 0.001$). (C) Expression of *noto* (shield-stage, a, b), *tbx6l* (60% epiboly, c, d), and *otx2* (100% epiboly stage, e, f) in WT and MZ*wnt8a* mutant embryos. Animal pole views with dorsal to the right (a, b). Lateral views with dorsal to the right (c-f). The lateral limits of *noto* expression are marked by arrows, the rostral and caudal limits of *otx2* expression are marked by arrowheads, and the ventral limit of *otx2* expression is marked by an asterisk. An expanded expression of *noto,* reduced expression of *tbx6l*, and expanded expression of *otx2* were observed in approximately half of the MZ mutant embryos (*noto*, n=28/65; *tbx6l*, n=13/26; *otx2*, n=13/28), compared to WT embryos (normal expression of *noto*, n=30/30; *tbx6l*, n=20/20; *otx2*, n=26/26). Scale bars: 500 μm in A; 200 μm in C.

**Fig. 5** Expression of Wnt ligand genes.

Semi-quantitative RT-PCR. Oocytes were harvested from WT or from two different female fish with *wnt8a*$^{\Delta O1\Delta O2/\Delta O1\Delta O2}$ germ cells (M*wnt8a* Female1/2), which were used to generate the M*wnt8a* and MZ*wnt8a* mutants in Fig. 3 and 4. RNA was isolated from the oocytes and 1-dpf WT embryos. The cDNA was generated from the same amount (1

μg) of RNAs in the presence (+) or absence (-) of reverse transcriptase (RT). The PCR conditions (amount of cDNA and PCR cycle number) were set to detect the expression of each *wnt* gene in 1-dpf WT embryos (see Material and methods). The PCR products were separated in agarose gels, and the black and white inverted images are shown. Among the *wnt* genes, the maternal expressions of *wnt6a* and *wnt8a* were stronger than their zygotic expression. *eef1a1l1* (formerly called *ef1a*) was analyzed as a control.

**Fig. 6** Wnt6a is another dorsal determinant candidate.

(A) Maternal expression of *wnt6a*. Whole-mount *in situ* hybridization of *wnt6a*, *wnt7ab,* and *wnt8* in one-cell-stage embryos. Staining with the sense probe for *wnt6a* was also performed as a negative control. *wnt6a* and *wnt8a* were detected in the vegetal pole (*wnt6a* antisense *n*=21/87, sense probe *n*=0/29; *wnt8a n*=18/19), whereas maternal *wnt7ab* was not detected (*n*=0/23). Lateral views. (B) Overexpression of *wnt6a* posteriorizes the embryos. One-cell-stage embryos were injected with the capped and polyadenylated RNA of *wnt6a* (5 pg), *wnt8a* (100 pg), *dkk1b* (50 pg), or a combination of *wnt6a* (5 pg) or *wnt8a* (100 pg), and *dkk1b* (50 pg). The phenotypes of the resultant embryos were observed at 30 hpf, and were categorized into four classes: no eyes, curled tail (a), no or small eyes (b), wild type-like (c), big head, short tail (d), and big head, no tail (e). Lateral views with anterior to the left. The proportion of embryos showing each phenotype is shown in the right panel. (C) Overexpression of *wnt6a* induces an expanded expression of *dharma*. The capped and polyadenylated RNA of *wnt6a* (1500 pg) or *wnt8a* (1500 pg) was injected into one-cell-stage embryos, and

*dharma* expression was examined at the sphere stage. Animal pole views with dorsal to the right (upper panels); lateral views with dorsal to the right (lower panels). The *dharma* expression was restricted to the dorsal-most region (*n*=20/20), whereas it was expanded in embryos that received an injection of *wnt6a* RNA (*n*=12/42) or *wnt8a* RNA (*n*=27/64). (D) Overexpression of Dkk1b, a canonical Wnt pathway inhibitor, suppressed the *dharma* expression. Embryos were injected with *dkk1b* RNA (375 or 1500 pg) or ΔN-*tcf7l1a* RNA (900 pg, formerly called ΔN-*tcf3a*). Lateral views with dorsal to the right. The *dharma* expression at the sphere stage was reduced in the embryos that received an injection of *dkk1b* RNA (*n*=13/35 for 375 pg; *n*=8/20 for 1500 pg) or ΔN-*tcf7l1a* RNA (*n*=32/37). Scale bars: 200 μm in A; 500 μm in B; 200 μm in C.

**Tables**

**Table 1** Relationship between genotype and no yolk extension phenotype in *wnt8a* mutants.

| *wnt8a* mutant allele | Genotype | Ratio of No-YE embryos |
|---|---|---|
| *ΔO1* | +/+ | 1/42 |
| | +/- | 3/93 |
| | -/- | 0/48 |
| *ΔO2* | +/+ | 0/17 |
| | +/- | 2/31 |
| | -/- | 2/22 |
| *ΔO1O2* | +/+ | 0/32 |
| | +/- | 0/73 |
| | -/- | 27/27 |
| *del* | +/+ | 0/11 |
| | +/- | 0/42 |
| | -/- | 17/17 |

Embryos were obtained by crossing heterozygote pairs of *wnt8a*$_{\Delta O1}$, *wnt8a*$_{\Delta O2}$, *wnt8a*$_{\Delta O1\Delta O2}$, and *wnt8a*$_{del}$ mutants. After phenotypic observation at 30 hpf, the genotype of each embryo was determined. The ratio of embryos showing the no-yolk extension phenotype is indicated.

**Legends for supplemental data**

**Fig. S1** *wnt8a* mutant alleles.

(A) Schematic of the *wnt8a* gene structure in zebrafish (same as in Fig. 1A). The position of the target regions of the TALENs is indicated by bars with T1 and T2. (B, C) Genomic sequence and protein structure of *wnt8a* mutants. The binding sites of the TALENs are indicated by boxes (T1-L/R, T2-L/R). Gray boxes indicate the insertion of non-relevant amino acids. (D) Detection of mutant alleles by genomic PCR. The PCR products were separated on acrylamide gels. The positions of a 100-bp marker (M) are indicated. For the *wnt8a*$_{del}$ allele, PCR primers detecting WT (upper panel) and the deletion alleles (lower panel) were designed separately. The mutant PCR products are indicated by asterisks. *wnt8a*$_{\Delta O1\text{-}1}$, *wnt8a*$_{\Delta O2\text{-}1}$, and *wnt8a*$_{\Delta O1\Delta O2\text{-}2}$ were representative of ORF1, ORF2, and ORF1/ORF2 mutants. The data from these mutants are shown in Fig. 2, 3, 4, Suppl. Fig. 5, and Table 1. The data of all of the *wnt8a* zygotic mutant phenotypes at 30 hpf are shown in Suppl. Fig. 2, 3, 4, and Suppl. Table 1, 2.

**Fig. S2.** Percentage of *wnt8a* mutants with the no-yolk-extension phenotype.

Embryos were obtained by crossing heterozygote pairs of WT, ORF1 (*ΔO1*), ORF2 (*ΔO2*), ORF1/ORF2 (*ΔO1ΔO2*), and deletion (*del*) mutants. The phenotypes were observed at 30 hpf. The embryos were categorized into two classes: normal and no yolk extension (No-YE). The numbers of observed embryos are indicated. About 25% of the embryos with mutations in both ORF1 and ORF2 showed the No-YE phenotype.

**Fig. S3.** Genotyping of *wnt8a* mutants.

Embryos were obtained by crossing heterozygote pairs of ORF1 (*ΔO1*, A), ORF2 (*ΔO2*, B), ORF1/ORF2 (*ΔO1ΔO2*, C), and deletion (*del*, D) mutants. After the phenotypic classification (normal or no yolk extension) at 30 hpf, the indicated numbers (in parenthesis) of embryos were genotyped. The percentage of embryos with each genotype is indicated.

**Fig. S4.** Antero-dorsalized phenotypes in the *wnt8a* ORF1/ORF2 mutants.

Embryos were obtained by crossing heterozygote pairs of *ΔO1ΔO2-1, ΔO1ΔO2-2, ΔO1ΔO2-3,* and *del* mutants. The phenotypes were analyzed at 30 hpf. The No-YE embryos were categorized into the three classes (C1-C3, in Fig. 2). The proportion of embryos showing of each phenotype class is indicated.

**Fig. S5.** *wnt8a* ORF1 mutants show a weak dorsalized phenotype.

(A) Expression of *noto* at the shield stage in *ΔO1* mutants. Embryos were obtained by crossing heterozygote pairs of WT, *ΔO1, ΔO2*, and *ΔO1ΔO2* mutants. Animal pole views with dorsal to the right. The homozygous embryos were identified by genotyping. The expression domain of *noto* was measured as an angle ($\theta$). (B) Expression domain of WT, *ΔO1, ΔO2*, and *ΔO1ΔO2* mutants. The averages are indicated by a line. Error bars indicate the standard error of the mean (SEM). Expression of *noto* was significantly expanded in the *ΔO1* and *ΔO1ΔO2* mutants (one-way ANOVA followed by Dunnet's post-hoc test, * $P < 0.05$, *** $P < 0.001$), although the expansion was much smaller in

the *ΔO1* mutants.

**Fig. S6.** Maternal zygotic *wnt8a*$^{\Delta O1\Delta O2\text{-}3}$ mutants show severe antero-dorsalized phenotypes.

An adult *wnt8a*$^{\Delta O1\Delta O2\text{-}3}$ homozygous female fish, which did not show any apparent phenotypes, was incidentally obtained. Embryos were obtained by crossing either *wnt8a*$^{\Delta O1\Delta O2\text{-}3}$ heterozygous male and female fish (het x het), or *wnt8a*$^{\Delta O1\Delta O2\text{-}3}$ homozygous female fish and heterozygous male fish (hom x het). The phenotypes were analyzed at 30 hpf. The percentage of embryos showing the no-yolk extension (No-YE) phenotype is indicated in (A). The No-YE embryos from “het x het” and “hom x het” were zygotic (Z) and maternal zygotic (MZ) *wnt8a* mutants, respectively. The proportion of No-YE embryos (Z*wnt8a* and MZ*wnt8a* mutants) of each phenotype class is indicated in (B). The proportions of C1-3 embryos were significantly different between the Z*wnt8a* and MZ*wnt8a* mutants (chi-square test, $P < 0.001$)

**Table S1.** Relationship between genotype and the no yolk extension phenotype in *wnt8a* mutants.

| *wnt8a* mutant allele | Total number | Embryos with normal YE | | | Embryos with no YE | | |
|---|---|---|---|---|---|---|---|
| | | +/+ | +/- | -/- | +/+ | +/- | -/- |
| *ΔO1-1* | 183 | 41 | 90 | 48 | 1 | 3 | 0 |
| *ΔO1-2* | 328 | 88 | 158 | 82 | 0 | 0 | 0 |
| *ΔO2-1* | 80 | 17 | 39 | 20 | 0 | 2 | 2 |
| *ΔO2-2* | 100 | 37 | 37 | 26 | 0 | 0 | 0 |
| *ΔO2-3* | 34 | 6 | 18 | 10 | 0 | 0 | 0 |
| *ΔO1ΔO2-1* | 132 | 32 | 73 | 0 | 0 | 0 | 27 |
| *ΔO1ΔO2-2* | 116 | 30 | 64 | 0 | 0 | 0 | 22 |
| *ΔO1ΔO2-3* | 174 | 40 | 89 | 0 | 0 | 0 | 45 |
| *del* | 70 | 11 | 42 | 0 | 0 | 0 | 17 |

Embryos were obtained by crossing heterozygote pairs of *ΔO1*, *ΔO2*, *ΔO1ΔO2*, and *del* mutants (all mutants described in Fig. S1). After the phenotypic observation at 30 hpf, the genotype of each embryo was determined. The numbers of observed embryos and of embryos showing each phenotype and genotype are indicated.

**Table S2.** Phenotypes of *wnt8a* compound mutants.

| *wnt8a* mutant alleles | | Number of embryos | | |
|---|---|---|---|---|
| Female | Male | Total | Normal | No-YE |
| *ΔO1*/+ | *ΔO2*/+ | 28 | 28 | 0 |
| *ΔO1*/*ΔO1* | *ΔO2*/+ | 139 | 135 | 4 |
| *ΔO1*/+ | *ΔO1ΔO2*/+ | 274 | 273 | 1 |
| *ΔO1*/*ΔO1* | *ΔO1ΔO2*/+ | 41 | 39 | 2 |
| *ΔO2*/+ | *ΔO1*/+ | 59 | 59 | 0 |
| *ΔO2*/*ΔO2* | *ΔO1*/+ | 188 | 186 | 2 |
| *ΔO2*/+ | *ΔO1ΔO2*/+ | 363 | 362 | 1 |
| *ΔO2*/*ΔO2* | *ΔO1ΔO2*/+ | 504 | 502 | 2 |

Embryos were obtained by crossing the indicated pairs of *wnt8a* mutant female and male fish. The total number of observed embryos and the number of embryos showing the normal or no-yolk extension phenotypes are indicated.

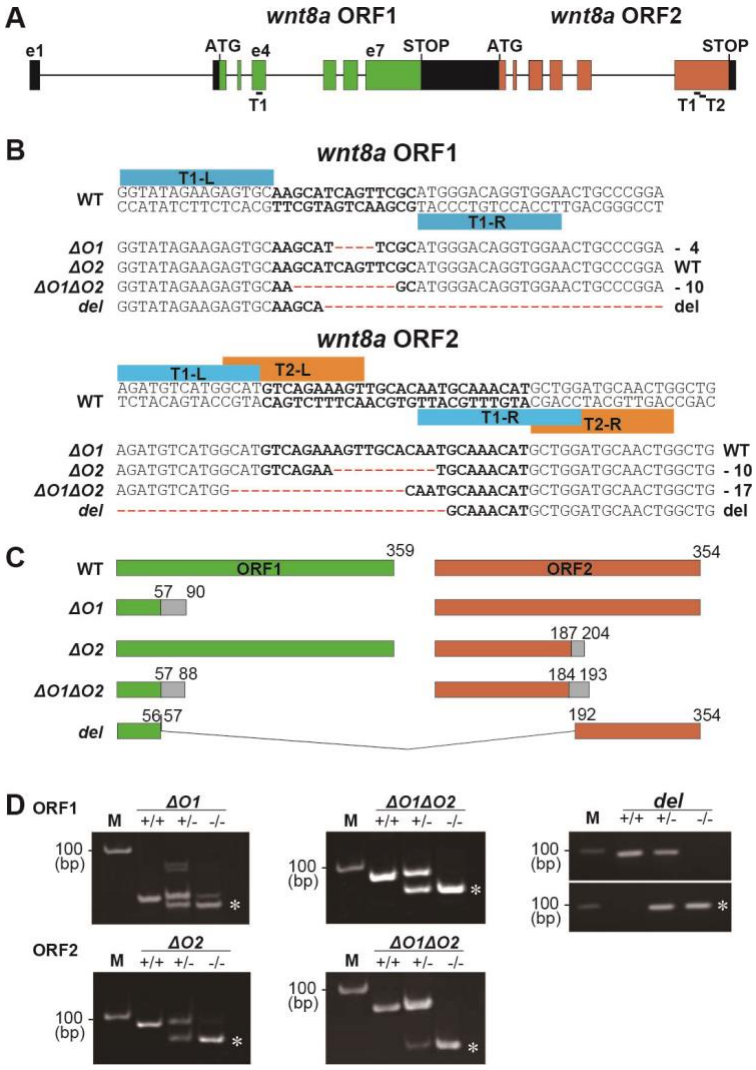


**Fig. 1** Generation of *wnt8a* mutants.
(A) Schematic of the *wnt8a* gene structure in zebrafish (to scale). Two ORFs (ORF1, ORF2) are tandemly located and encode two Wnt8a proteins. The 5' and 3' non-coding exons are indicated by black boxes, and ORF1 and ORF2 by green and orange boxes, respectively. The positions of the translational initiation sites and stop codons are indicated. The position of the target regions of the TALENs is indicated by bars with T1 and T2. (B, C) *wnt8a*$_{\Delta O1}$, *wnt8a*$_{\Delta O2}$, *wnt8a*$_{\Delta O1\Delta O2}$, and *wnt8a*$_{del}$ mutants generated by TALENs. One and two sets of TALENs were generated and used to introduce mutations in ORF1 (T1) and ORF2 (T1 and T2), respectively. Two and three mutants had an indel mutation in ORF1 (*ΔO1-1,2*) or ORF2 (*ΔO2-1,2,3*), respectively; three mutants had indel mutations in both ORF1 and ORF2 (*ΔO1ΔO2-1,2,3*); and one mutant had a long deletion in the ORF1/ORF2 region (*del*). Partial sequences of the *wnt8a* ORF1 and ORF2 genes in wild-type (WT) and a typical mutant from each group (*ΔO1-1, ΔO2-1, ΔO1ΔO2-2*, and *del*) are shown in (B). These mutants were used for the analyses shown in Fig. 2, 3, 4, and Suppl. Fig. 5. The sequence information of all of the *wnt8a* mutants is shown in Suppl. Fig. 1. The binding sites of the TALENs are indicated by boxes with T1-L/R or T2-L/R (B). The putative protein structures from the WT and mutant genes (*ΔO1*, *ΔO2*, *ΔO1ΔO2*, and *del*) are shown in (C). Gray boxes indicate an insertion of non-relevant amino acids. (D) Detection of the mutant alleles by genomic PCR. The PCR products were separated by acrylamide gel electrophoresis. The positions of a 100-bp marker (M) are indicated. The mutant PCR products are indicated by asterisks. Although a band was seen at the position of the wild-type ORF1 PCR product in the *ΔO1* homozygous mutant, it was non-specific, since it was also detected in the *del* mutants. For the *wnt8a*$_{del}$ allele, PCR primers detecting the WT (upper panel) and the deletion allele (lower panel) were designed separately.

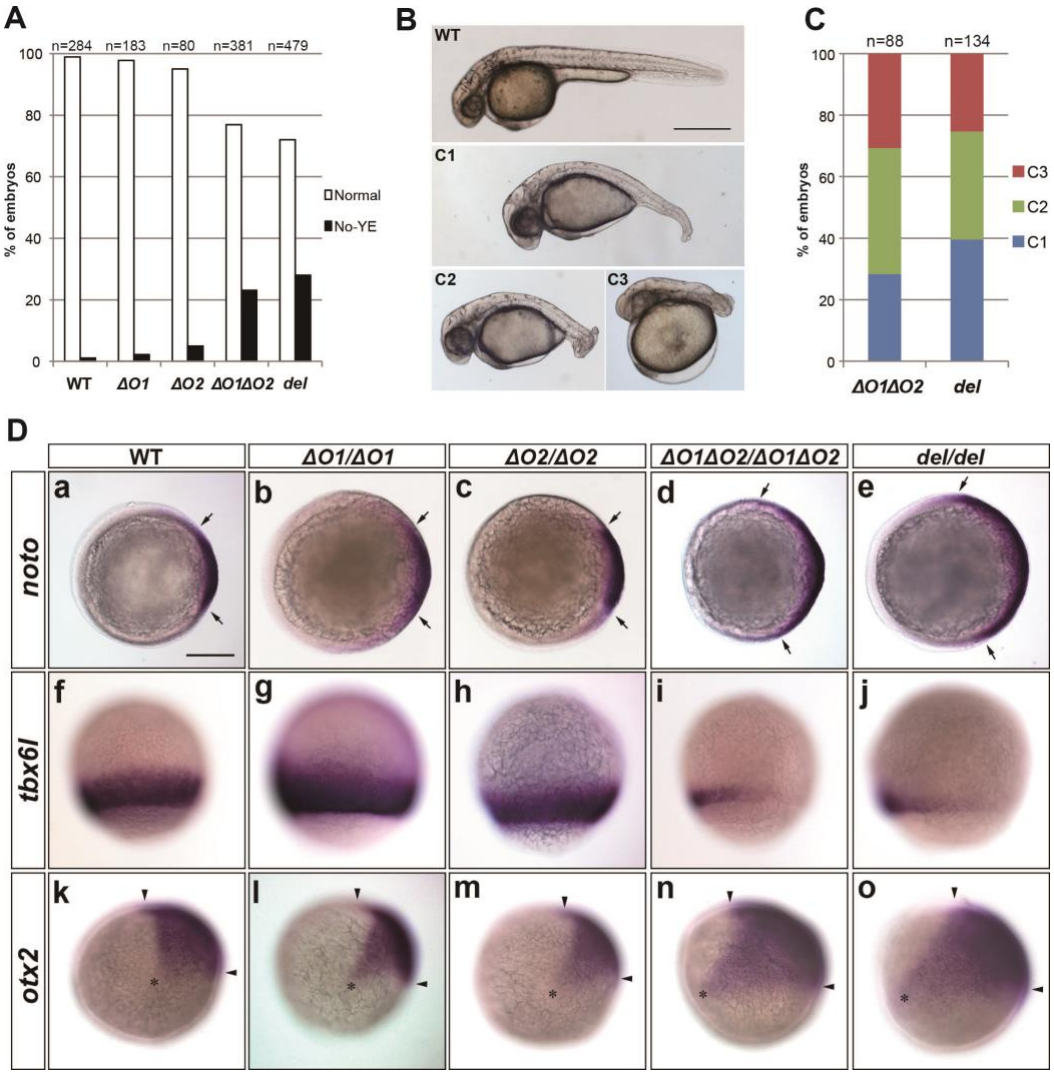


**Fig. 2** Role of ORF1 and ORF2 in the zygotic *wnt8a*-mediated development of caudal and ventrolateral tissues.
(A) Percentage of mutants showing a lack of yolk extension (no yolk extension: No-YE). Embryos were obtained by crossing WT, or *wnt8a*$_{\Delta O1}$(*ΔO1*), *wnt8a*$_{\Delta O2}$ (*ΔO2*), *wnt8a*$_{\Delta O1\Delta O2}$ (*ΔO1ΔO2*), or *wnt8a*$_{del}$ (*del*) heterozygote pairs. Phenotypes were observed at 30 hpf. The number of observed embryos is indicated. (B) WT and *wnt8a* mutant phenotypes. Lateral views with anterior to the left. The No-YE embryos were categorized into three classes. C1 embryos had a slightly shortened and ventrally bent tail, C2 embryos had a short and curled tail, and C3 embryos had an enlarged head and a truncated tail. This phenotype classification is essentially the same as one described in a previous publication (Shimizu et al., 2005), except for being based on the No-YE phenotype. (C) Proportion of No-YE embryos showing each phenotype class. The number of observed embryos is indicated. (D) Expression of *noto* (formerly called *floating head*, shield stage, a-e), *tbx6l* (*tbx6*, 80% epiboly stage, f-j), and *otx2* (100% epiboly stage, k-o) in WT (a, f, k) and *ΔO1* (b, g, l), *ΔO2* (c, h, m), *ΔO1ΔO2* (d, i, n), and *del* (e, j, o) homozygous mutants. Animal pole views with dorsal to the right (a-e). Lateral views with dorsal to the right (f-o). *noto*, *tbx6l*, and *otx2* are markers of the axial mesoderm, the paraxial mesoderm, and the rostral neuroectoderm (forebrain and midbrain), respectively. The lateral limits of *noto* expression are marked by arrows, the rostral and caudal limits of *otx2* expression are marked by arrowheads, and the ventral limit of *otx2* expression is marked by an asterisk. The *noto* expression was not greatly affected in the *ΔO1* and *ΔO2* single mutants, but it was prominently expanded in the *ΔO1ΔO2* and *del* mutants (*ΔO1*, n=0/86; *ΔO2*, n=0/94; *ΔO1ΔO2*, n=10/42; *del*, n=15/44 in embryos from the heterozygous crosses; *ΔO1*, n=0/7; *ΔO2*, n=0/7; *ΔO1ΔO2*, n=4/4; *del*, n=6/6 in genotyped homozygotes). The *tbx6l* expression was not affected in the *ΔO1* or *ΔO2* mutants, but was reduced or absent in the *ΔO1ΔO2* and *del* mutants (*ΔO1*, n=0/353; *ΔO2*, n=0/96; *ΔO1ΔO2*, n=27/83; *del*, n=37/140 in embryos from the heterozygous crosses; *ΔO1*, n=0/22; *ΔO2*, n=0/9; *ΔO1ΔO2*, n=11/11; *del*, n=10/10 in the genotyped homozygotes). The *otx2* expression was not affected in the *ΔO1* or *ΔO2* mutants, but was expanded in the *ΔO1ΔO2* and *del* mutants (*ΔO1*, n=0/73; *ΔO2*, n=0/99; *ΔO1ΔO2*, n=10/49; *del*, n=18/57 in embryos from the heterozygous crosses; *ΔO1*, n=0/6; *ΔO2*, n=0/7; *ΔO1ΔO2*, n=6/6; *del*, n=6/6 in genotyped homozygotes). Scale bars: 500 μm in B; 200 μm in D.

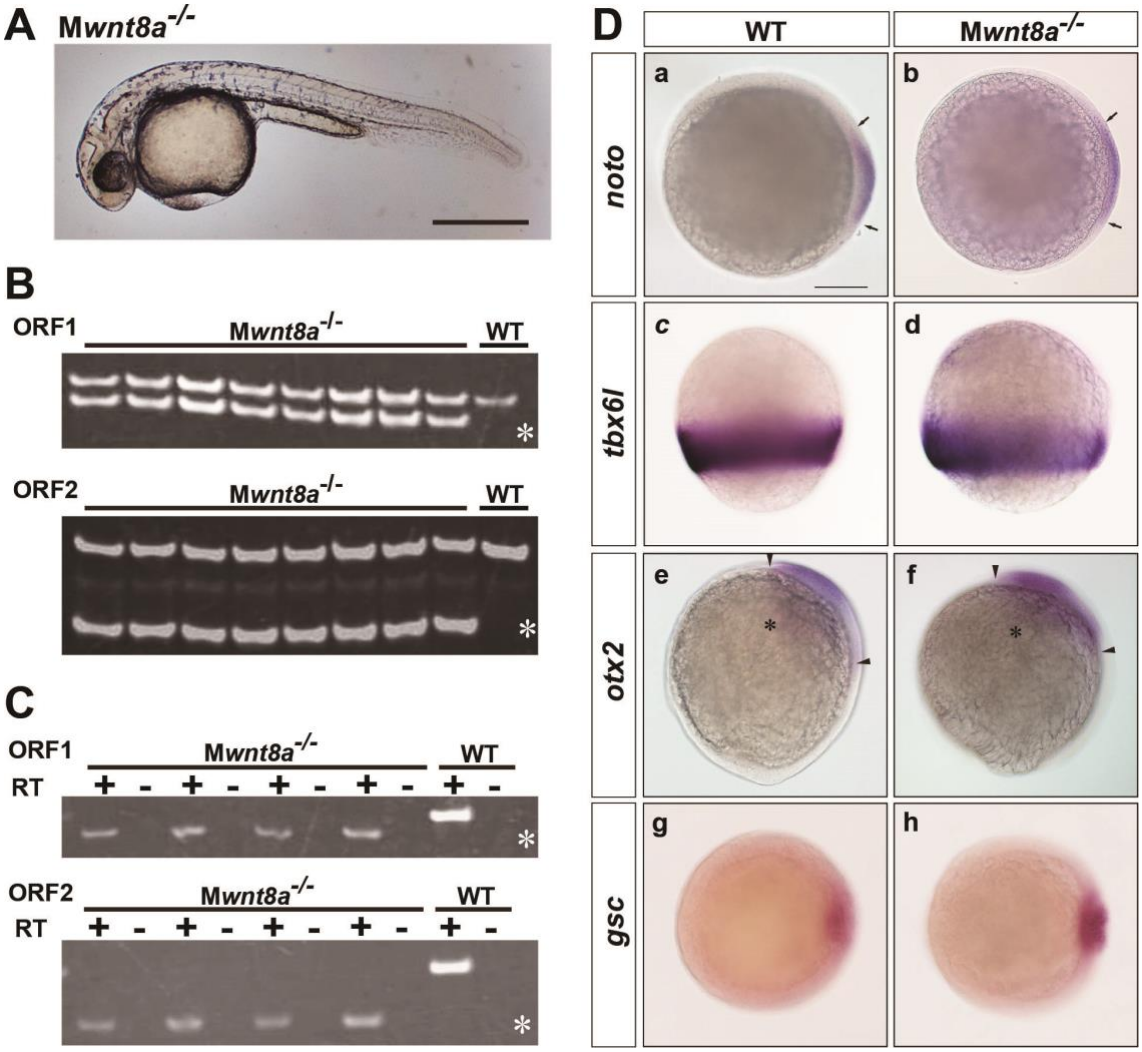


**Fig. 3** Maternal *wnt8a* mutants show no defects in dorsal-axis formation.
(A) Maternal *wnt8a* mutant embryos (M*wnt8a*$^{-/-}$) at 30 dpf. Embryos were obtained by crossing WT male fish and female fish with *wnt8a*$^{\Delta O1\Delta O2/\Delta O1\Delta O2}$ germ cells. Lateral view with anterior to the left. The M*wnt8a*$^{-/-}$ mutant embryos showed no apparent abnormality in dorsal axis formation (*n*=190). (B, C) Genotyping and RT-PCR of M*wnt8* mutant embryos. The TALEN target regions of ORF1 (upper panel) and ORF2 (lower panel) were amplified by PCR from the genome of a WT and eight M*wnt8a* mutant embryos (B), and by RT-PCR from the RNA of a one-cell-stage WT and four M*wnt8a* mutant embryos (C). The PCR products were separated on acrylamide gels. The positions of the PCR bands corresponding to the mutant DNAs are marked by asterisks. "+" and "-" indicate the presence and absence of reverse transcriptase (RT) in the cDNA synthesis. Note that all of the M*wnt8a* mutant embryos had both WT and mutant alleles (*n*=8/8), and all four M*wnt8a* mutants had only mutant ORF1 and ORF2 transcripts. (D) Expression of *noto* (shield stage, a, b), *tbx6l* (80% epiboly stage, c, d), *otx2* (100% epiboly stage, e, f), and *gsc* (shield stage, g, h) in WT and M*wnt8a* mutants. M*wnt8a* mutants were obtained by crossing female fish with *wnt8a*$^{\Delta O1\Delta O2/\Delta O1\Delta O2}$ germ cells and WT (b, d, f) or *wnt8a*$^{\Delta O1\Delta O2/+}$ male (h) fish. Animal pole views with dorsal to the right (a, b, g, h). Lateral views with dorsal to the right (c-f). The expression of *noto*, *tbx6l*, *otx2*, and *gsc* was unaffected in the M*wnt8a* mutants compared to WT embryos (*noto*, n=20; *tbx6l*, n=20; *otx2*, n=20; *gsc*, n=16). Scale bars: 500 μm in A; 200 μm in D.

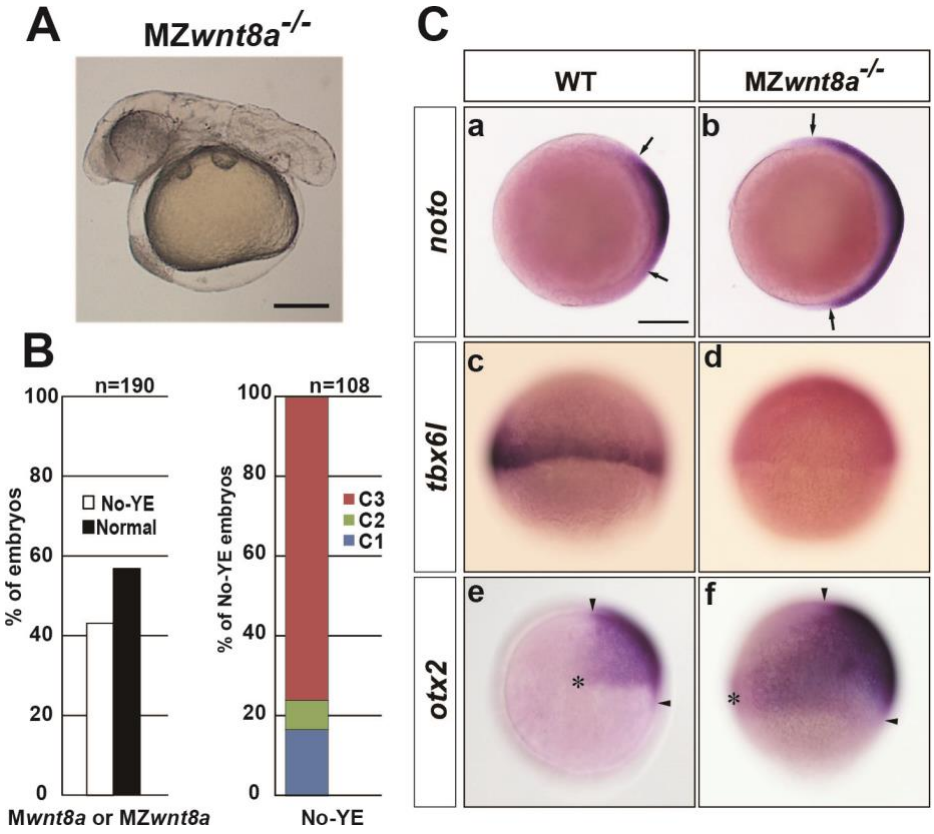


**Fig. 4** Maternal *wnt8a* supports the functions of zygotic *wnt8a*.
(A) Phenotype of maternal-zygotic *wnt8a* mutant (MZ*wnt8a*$^{-/-}$) embryos at 30 hpf. Embryos were obtained by crossing *wnt8a*$^{\Delta O1\Delta O2/+}$ male fish and female fish with *wnt8a*$^{\Delta O1\Delta O2/\Delta O1\Delta O2}$ germ cells. Lateral view with anterior to the left. Approximately half of the embryos were predicted to be MZ*wnt8a*$^{-/-}$ embryos, and the rest were M*wnt8a*$^{-/-}$ embryos. The MZ*wnt8a*$^{-/-}$ embryos were identified by genotyping. (B) Percentage of embryos showing the no-yolk extension phenotype (No-YE, left panel), and of No-YE embryos showing the antero-dorsalized phenotypes C1-3 (right panel, Fig. 2B). MZ*wnt8a* showed more severe antero-dorsalized phenotypes than did zygotic (Z) *wnt8a* mutants (*ΔO1ΔO2* in Fig. 2C). The proportions of C1-3 embryos were significantly different between the Z*wnt8a* and MZ*wnt8a* mutants (chi-square test, $P < 0.001$). (C) Expression of *noto* (shield-stage, a, b), *tbx6l* (60% epiboly, c, d), and *otx2* (100% epiboly stage, e, f) in WT and MZ*wnt8a* mutant embryos. Animal pole views with dorsal to the right (a, b). Lateral views with dorsal to the right (c-f). The lateral limits of *noto* expression are marked by arrows, the rostral and caudal limits of *otx2* expression are marked by arrowheads, and the ventral limit of *otx2* expression is marked by an asterisk. An expanded expression of *noto,* reduced expression of *tbx6l*, and expanded expression of *otx2* were observed in approximately half of the MZ mutant embryos (*noto*, n=28/65; *tbx6l*, n=13/26; *otx2*, n=13/28), compared to WT embryos (normal expression of *noto*, n=30/30; *tbx6l*, n=20/20; *otx2*, n=26/26). Scale bars: 500 μm in A; 200 μm in C.

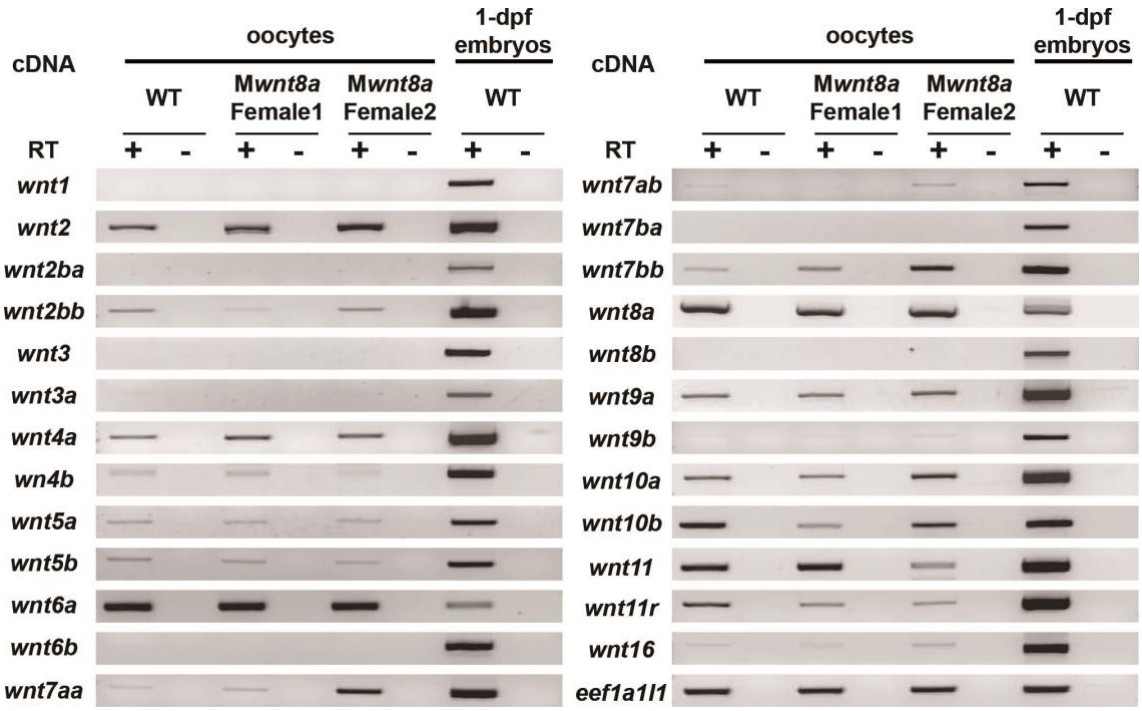


**Fig. 5** Expression of Wnt ligand genes.
Semi-quantitative RT-PCR. Oocytes were harvested from WT or from two different female fish with *wnt8a*$^{\Delta O1\Delta O2/\Delta O1\Delta O2}$ germ cells (M*wnt8a* Female1/2), which were used to generate the M*wnt8a* and MZ*wnt8a* mutants in Fig. 3 and 4. RNA was isolated from the oocytes and 1-dpf WT embryos. The cDNA was generated from the same amount (1 μg) of RNAs in the presence (+) or absence (-) of reverse transcriptase (RT). The PCR conditions (amount of cDNA and PCR cycle number) were set to detect the expression of each *wnt* gene in 1-dpf WT embryos (see Material and methods). The PCR products were separated in agarose gels, and the black and white inverted images are shown. Among the *wnt* genes, the maternal expressions of *wnt6a* and *wnt8a* were stronger than their zygotic expression. *eef1a1l1* (formerly called *ef1a*) was analyzed as a control.

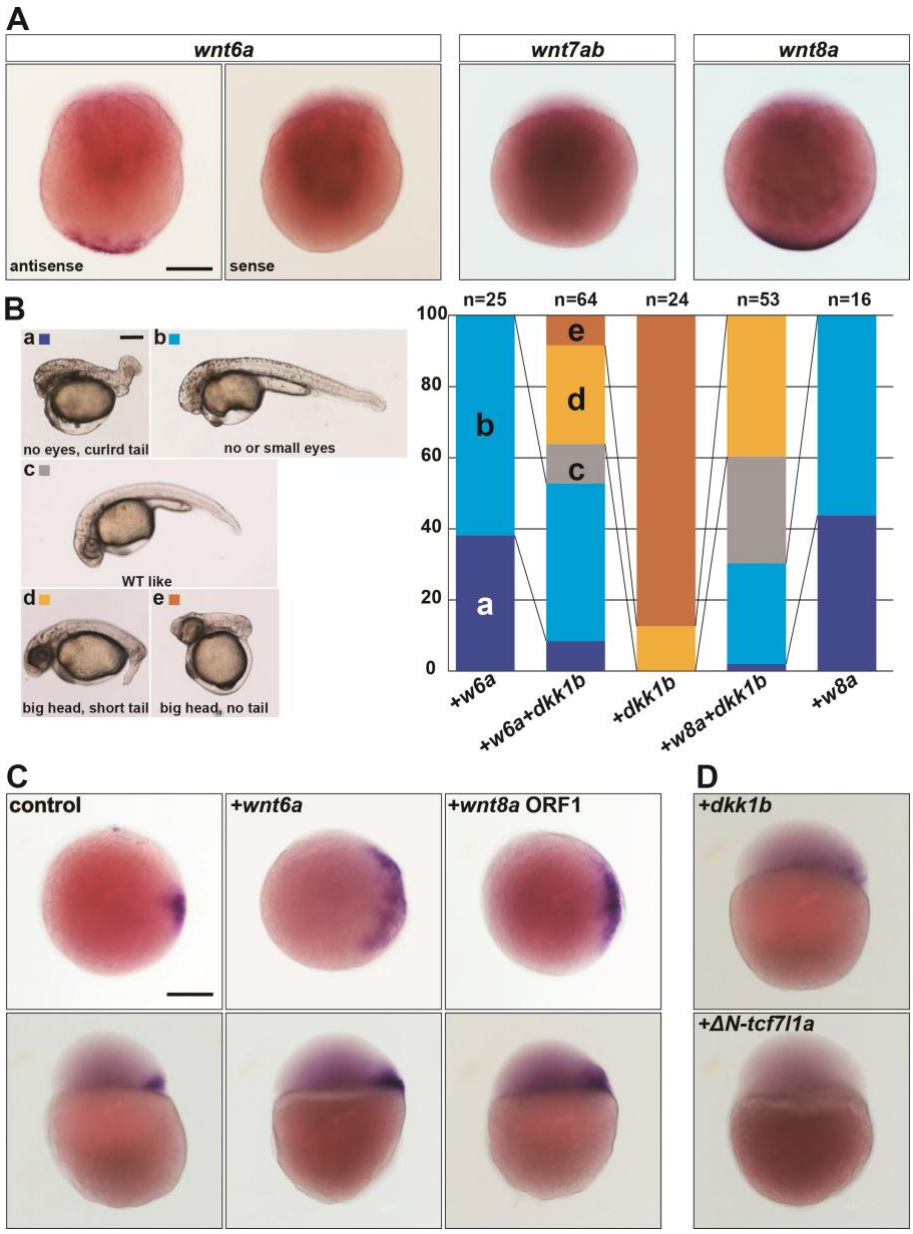


**Fig. 6** Wnt6a is another dorsal determinant candidate.
(A) Maternal expression of *wnt6a*. Whole-mount *in situ* hybridization of *wnt6a*, *wnt7ab,* and *wnt8* in one-cell-stage embryos. Staining with the sense probe for *wnt6a* was also performed as a negative control. *wnt6a* and *wnt8a* were detected in the vegetal pole (*wnt6a* antisense *n*=21/87, sense probe *n*=0/29; *wnt8a n*=18/19), whereas maternal *wnt7ab* was not detected (*n*=0/23). Lateral views. (B) Overexpression of *wnt6a* posteriorizes the embryos. One-cell-stage embryos were injected with the capped and polyadenylated RNA of *wnt6a* (5 pg), *wnt8a* (100 pg), *dkk1b* (50 pg), or a combination of *wnt6a* (5 pg) or *wnt8a* (100 pg), and *dkk1b* (50 pg). The phenotypes of the resultant embryos were observed at 30 hpf, and were categorized into four classes: no eyes, curled tail (a), no or small eyes (b), wild type-like (c), big head, short tail (d), and big head, no tail (e). Lateral views with anterior to the left. The proportion of embryos showing each phenotype is shown in the right panel. (C) Overexpression of *wnt6a* induces an expanded expression of *dharma*. The capped and polyadenylated RNA of *wnt6a* (1500 pg) or *wnt8a* (1500 pg) was injected into one-cell-stage embryos, and *dharma* expression was examined at the sphere stage. Animal pole views with dorsal to the right (upper panels); lateral views with dorsal to the right (lower panels). The *dharma* expression was restricted to the dorsal-most region (*n*=20/20), whereas it was expanded in embryos that received an injection of *wnt6a* RNA (*n*=12/42) or *wnt8a* RNA (*n*=27/64). (D) Overexpression of Dkk1b, a canonical Wnt pathway inhibitor, suppressed the *dharma* expression. Embryos were injected with *dkk1b* RNA (375 or 1500 pg) or ΔN-*tcf7l1a* RNA (900 pg, formerly called ΔN-*tcf3a*). Lateral views with dorsal to the right. The *dharma* expression at the sphere stage was reduced in the embryos that received an injection of *dkk1b* RNA (*n*=13/35 for 375 pg; *n*=8/20 for 1500 pg) or ΔN-*tcf7l1a* RNA (*n*=32/37). Scale bars: 200 μm in A; 500 μm in B; 200 μm in C.

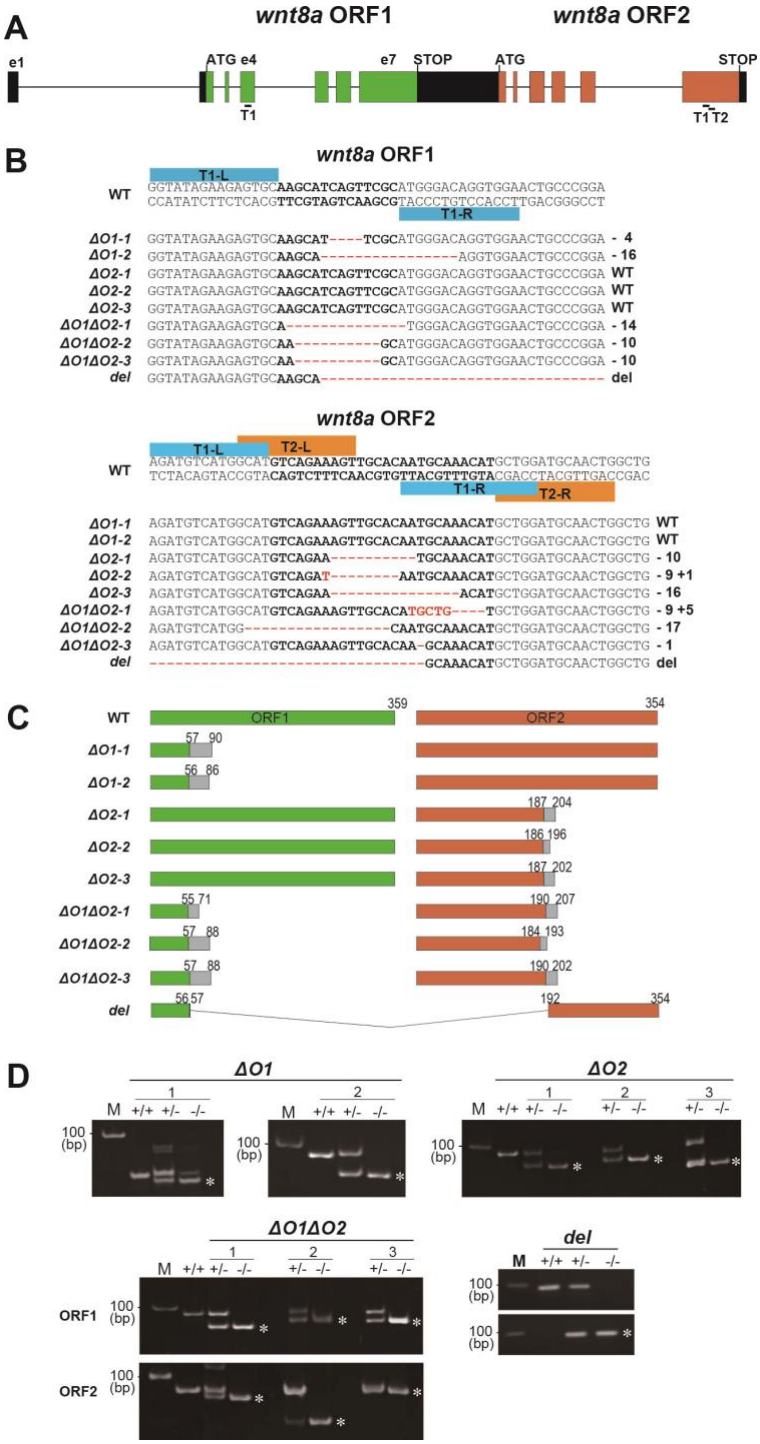


**Fig. S1** *wnt8a* mutant alleles.
(A) Schematic of the *wnt8a* gene structure in zebrafish (same as in Fig. 1A). The position of the target regions of the TALENs is indicated by bars with T1 and T2. (B, C) Genomic sequence and protein structure of *wnt8a* mutants. The binding sites of the TALENs are indicated by boxes (T1-L/R, T2-L/R). Gray boxes indicate the insertion of non-relevant amino acids. (D) Detection of mutant alleles by genomic PCR. The PCR products were separated on acrylamide gels. The positions of a 100-bp marker (M) are indicated. For the *wnt8a*$^{del}$ allele, PCR primers detecting WT (upper panel) and the deletion alleles (lower panel) were designed separately. The mutant PCR products are indicated by asterisks. *wnt8a*$^{\Delta O1\text{-}1}$, *wnt8a*$^{\Delta O2\text{-}1}$, and *wnt8a*$^{\Delta O1\Delta O2\text{-}2}$ were representative of ORF1, ORF2, and ORF1/ORF2 mutants. The data from these mutants are shown in Fig. 2, 3, 4, Suppl. Fig. 5, and Table 1. The data of all of the *wnt8a* zygotic mutant phenotypes at 30 hpf are shown in Suppl. Fig. 2, 3, 4, and Suppl. Table 1, 2.

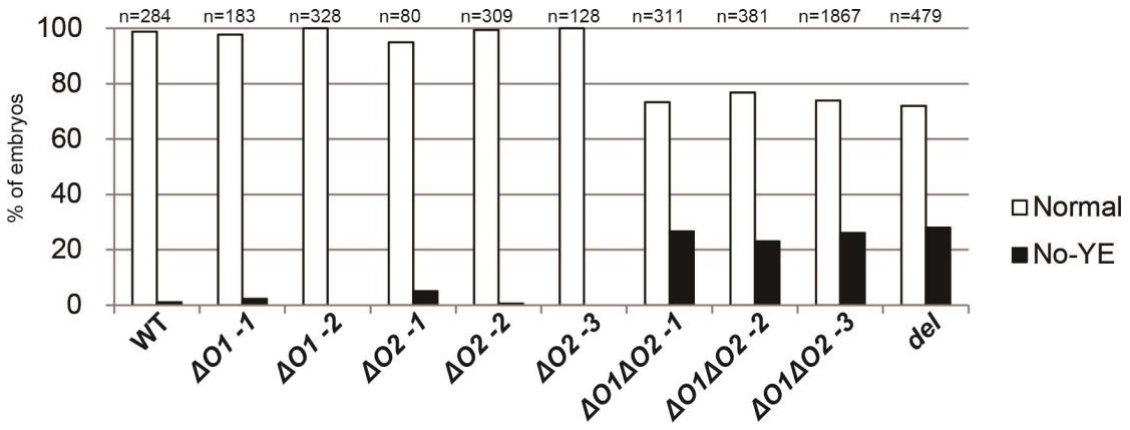


**Fig. S2.** Percentage of *wnt8a* mutants with the no-yolk-extension phenotype.
Embryos were obtained by crossing heterozygote pairs of WT, ORF1 (*ΔO1*), ORF2 (*ΔO2*), ORF1/ORF2 (*ΔO1ΔO2*), and deletion (*del*) mutants. The phenotypes were observed at 30 hpf. The embryos were categorized into two classes: normal and no yolk extension (No-YE). The numbers of observed embryos are indicated. About 25% of the embryos with mutations in both ORF1 and ORF2 showed the No-YE phenotype.

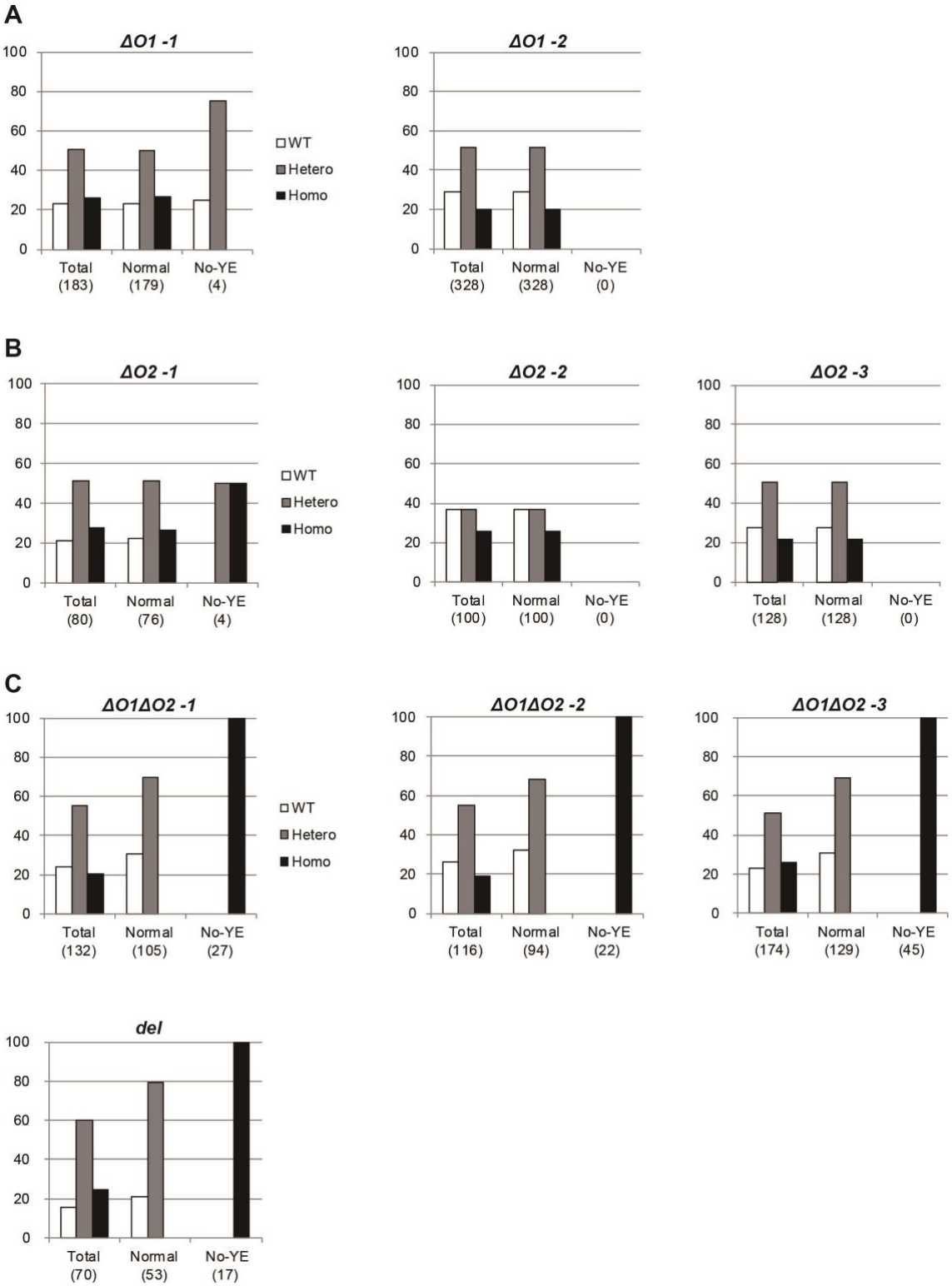


**Fig. S3.** Genotyping of *wnt8a* mutants.
Embryos were obtained by crossing heterozygote pairs of ORF1 (*ΔO1*, A), ORF2 (*ΔO2*, B), ORF1/ORF2 (*ΔO1ΔO2*, C), and deletion (*del*, D) mutants. After the phenotypic classification (normal or no yolk extension) at 30 hpf, the indicated numbers (in parenthesis) of embryos were genotyped. The percentage of embryos with each genotype is indicated.

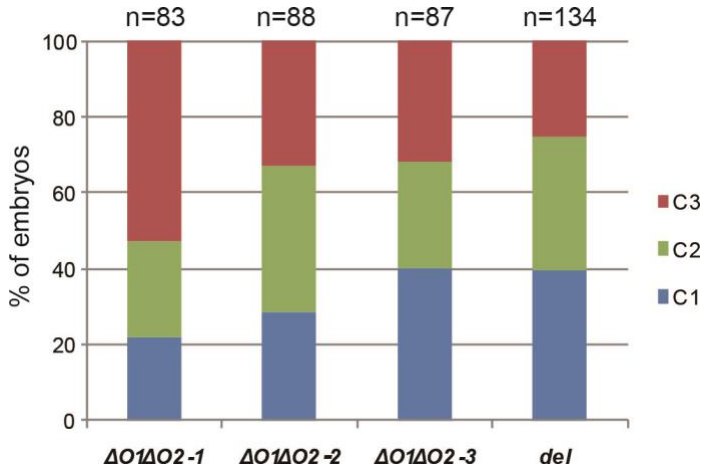


**Fig. S4.** Antero-dorsalized phenotypes in the *wnt8a* ORF1/ORF2 mutants.
Embryos were obtained by crossing heterozygote pairs of *ΔO1ΔO2-1, ΔO1ΔO2-2, ΔO1ΔO2-3,* and *del* mutants. The phenotypes were analyzed at 30 hpf. The No-YE embryos were categorized into the three classes (C1-C3, in Fig. 2). The proportion of embryos showing of each phenotype class is indicated.

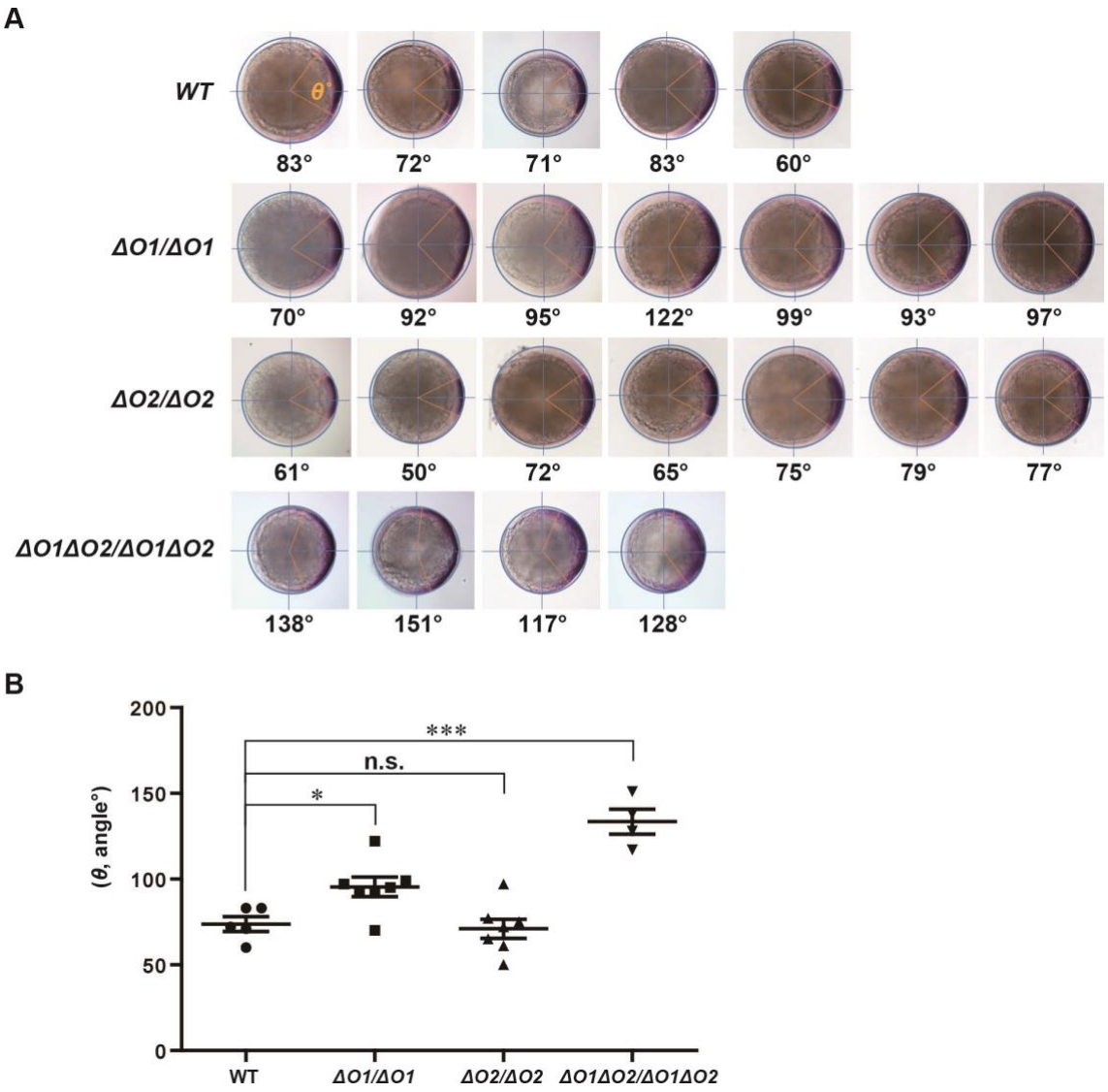


**Fig. S5.** *wnt8a* ORF1 mutants show a weak dorsalized phenotype.

(A) Expression of *noto* at the shield stage in *ΔO1* mutants. Embryos were obtained by crossing heterozygote pairs of WT, *ΔO1, ΔO2*, and *ΔO1ΔO2* mutants. Animal pole views with dorsal to the right. The homozygous embryos were identified by genotyping. The expression domain of *noto* was measured as an angle ($\theta$). (B) Expression domain of WT, *ΔO1, ΔO2*, and *ΔO1ΔO2* mutants. The averages are indicated by a line. Error bars indicate the standard error of the mean (SEM). Expression of *noto* was significantly expanded in the *ΔO1* and *ΔO1ΔO2* mutants (one-way ANOVA followed by Dunnet's post-hoc test, * $P < 0.05$, *** $P < 0.001$), although the expansion was much smaller in the *ΔO1* mutants.

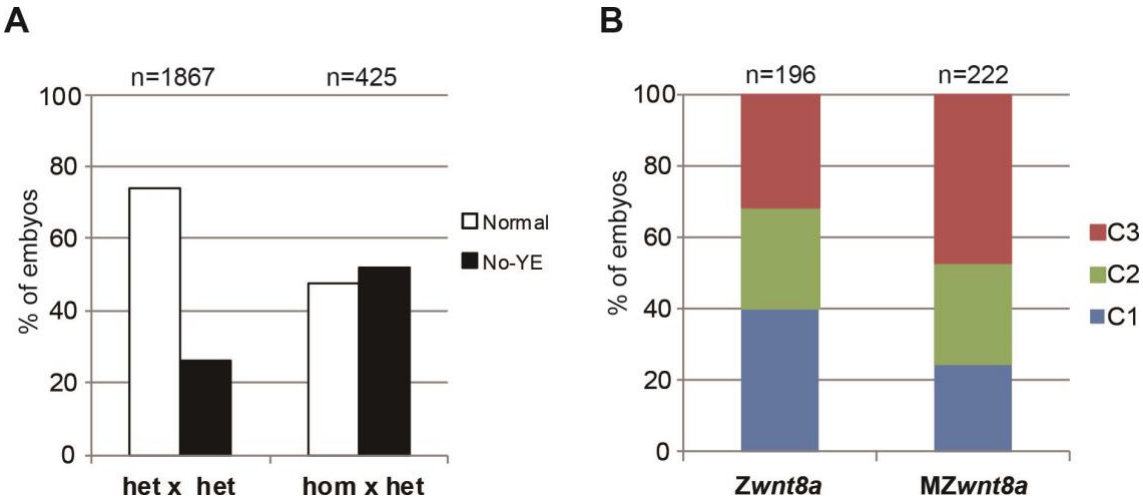


**Fig. S6.** Maternal zygotic *wnt8a*$^{\Delta O1\Delta O2\text{-}3}$ mutants show severe antero-dorsalized phenotypes.
An adult *wnt8a*$^{\Delta O1\Delta O2\text{-}3}$ homozygous female fish, which did not show any apparent phenotypes, was incidentally obtained. Embryos were obtained by crossing either *wnt8a*$^{\Delta O1\Delta O2\text{-}3}$ heterozygous male and female fish (het x het), or *wnt8a*$^{\Delta O1\Delta O2\text{-}3}$ homozygous female fish and heterozygous male fish (hom x het). The phenotypes were analyzed at 30 hpf. The percentage of embryos showing the no-yolk extension (No-YE) phenotype is indicated in (A). The No-YE embryos from "het x het" and "hom x het" were zygotic (Z) and maternal zygotic (MZ) *wnt8a* mutants, respectively. The proportion of No-YE embryos (Z*wnt8a* and MZ*wnt8a* mutants) of each phenotype class is indicated in (B). The proportions of C1-3 embryos were significantly different between the Z*wnt8a* and MZ*wnt8a* mutants (chi-square test, $P < 0.001$).